CHALMERS
UNIVERSITY OF TECHNOLOGY

Model reduction of finite element models applied to nonlinear squeak and rattle simulation

Master's thesis in Applied Mechanics

ANOOB VALIYAKATH BASHEER
FILIP GODBORG

Department of Mechanics and Maritime Sciences
CHALMERS UNIVERSITY OF TECHNOLOGY
Gothenburg, Sweden 2019

Master's thesis 2019:21

Model reduction of finite element models applied to nonlinear squeak and rattle simulation

ANOOB VALIYAKATH BASHEER
FILIP GODBORG

CHALMERS
UNIVERSITY OF TECHNOLOGY

Department of Mechanics and Maritime Sciences
Chalmers University of Technology
Gothenburg, Sweden 2019

Model reduction of finite element models applied to nonlinear squeak and rattle simulation
ANOOB VALIYAKATH BASHEER
FILIP GODBORG

Master's Thesis 2019:21
Department of Mechanics and Maritime Sciences
Chalmers University of Technology
SE-412 96 Gothenburg
Telephone +46 31 772 1000

Model reduction of finite element models applied to nonlinear squeak and rattle simulation

ANOOB VALIYAKATH BASHEER
FILIP GODBORG
Department of Mechanics and Maritime Sciences
Chalmers University of Technology

Abstract

High level of modelling details in finite element models contributes to an increase in computational cost. To deal with this, the Component Mode Synthesis can be used, which combines the principle of dynamic substructuring with techniques of model reduction. The most common Component Mode Synthesis method is the Craig-Bampton method that has been labeled as the standard method for dynamic substructuring of linear systems. However, for dynamic substructuring of nonlinear systems, no standard method has emerged as the research within the area is still at an early stage. Hence, it would be beneficial to investigate if the Craig-Bampton method can be used for squeak and rattle simulations including nonlinearities in the form of contact.

This thesis aims to increase the understanding of how the Craig-Bampton method can be used for simulations including nonlinearities in the form of contact. The study is carried out on a passenger car door which is excited using three different load cases, to see the influence of different levels of contact. The substructured model is compared to the original model by using the Modal Assurance Criterion, frequency response comparison and by comparing contact force with respect to time and amplitude. Further, by gradually excluding more elements from the substructure, the thesis aims to see if the accuracy of squeak and rattle prediction can be improved by having a higher number of elements closer to the contact region.

The results show that the substructured system had 97.9 % lower computational time than the original FE-model. Although it was accurate at predicting contact with respect to time, the calculated contact force amplitudes were generally higher. Neither the level of contact nor the number of elements close to the contact region had any significant effect for squeak and rattle prediction of the substructured model. The computational time is found to be dominated by the number of interface DOFs. In this case, an additional 32.5 % reduction in computational time was achieved by locally coarsening the mesh around the contact interface.

Keywords: Component Mode Synthesis, Craig-Bampton, model reduction, Guyan reduction, nonlinearity, Modal Assurance Criterion

Acknowledgements

We would like to thank our supervisors Mohsen Bayani and Mladen Gibanica for the support and guidance during this thesis. Their expertise and willingness to continuously help has been a great source for knowledge and motivation.

We would also like to thank our examiner Thomas Abrahamsson, professor in structural dynamics, for the opportunity of doing this thesis. With his expertise, Thomas has given new interesting perspectives to the thesis.

A special thank you also to Henrik Viktorsson, CAE engineer at Volvo Cars, for the CAE-support during this thesis. Finally, we would like to thank the people at the Solidity group who helped us achieving this thesis work.

Authors, May 2019

Nomenclature

Abbreviations:
S&R - Squeak and rattle
VCC - Volvo Car Corporation
CAE - Computer aided engineering
CMS - Component mode synthesis
DOF - Degree-of-freedom
DOFs - Degrees-of-freedom
FE - Finite element
FFT - Fast Fourier transform
IFFT - Inverse fast Fourier transform
MAC - Modal assurance criterion
FEM - Finite element method
FEA - Finite element analysis
StS - Surface-to-surface
NtS - Node-to-surface
rDOF - retained degree-of-freedom
rDOFs - retained degrees-of-freedom

Symbols:
$\boldsymbol{M}$ - Mass matrix [kg]
$\boldsymbol{K}$ - Stiffness matrix [N/m]
$\boldsymbol{q}$ - Displacement [m]
ω - Angular frequency [rad/s]
$\boldsymbol{x}$ - Eigenvector
H - Transfer function [-]
F - Force [N]
Ψ_c - Guyan mode matrix
Φ_i - Fixed interface vibration mode matrix
Ψ_{CB} - Craig-Bampton reduction matrix
$\boldsymbol{\eta}$ - Vector of modal degrees-of-freedom
$\boldsymbol{M}_{CB}$ - Reduced mass matrix [kg]
$\boldsymbol{K}_{CB}$ - Reduced stiffness matrix [N/m]
$\boldsymbol{F}_{CB}$ - Reduced force vector [N]
π_c - Contact energy function
g_N - Normal gap between contact surfaces
κ - Large number
- Number of

Subscripts:
i - Internal degree-of-freedom
b - Boundary degree-of-freedom
r - Reference data set
r,m - mean value of reference data set

Contents

List of Figures

List of Tables

1
Introduction

1.1 Background

Squeak and rattle (S&R) are two types of noises that are induced during the car operational states, and many drivers perceive it as irritating, distracting and as a sign of poor quality. Figure 1.1 visualises the two scenarios of S&R, where two adjacent parts are impacting on each other. The left figure visualises the rattle phenomena where the parts are impacting on each other in the normal direction. The right figure visualises the squeak phenomena where the parts are sliding relative to one another. The solidity group at Volvo Car Corporation (VCC) is making a great effort to counteract these problems, which is advantageous to do in a phase prior to manufacturing. To this end, Computer-aided engineering (CAE) can be used to locate problematic areas before manufacturing. It accelerates S&R verification and reduces the need for expensive and time-consuming physical tests.

One step towards improving the CAE process is to create more accurate CAE models by including a high level of modelling details. However, this contributes to an increased computational cost, which reduces the efficiency of the CAE process. The Component Mode Synthesis (CMS) method is commonly used to deal with this problem in linear analyses [1]. The CMS method combines the principle of dynamic substructuring with the techniques of model reduction. The method reduces the number of degrees-of-freedom (DOFs), making the model smaller and more efficient to solve. The automotive industry already uses well-established CMS methods for linear problems, such as the Craig-Bampton method, which has been used since the 1960s [2]. It has been labeled as the standard method for dynamic substructuring of linear systems. However, for dynamic substructuring of nonlinear problems, there

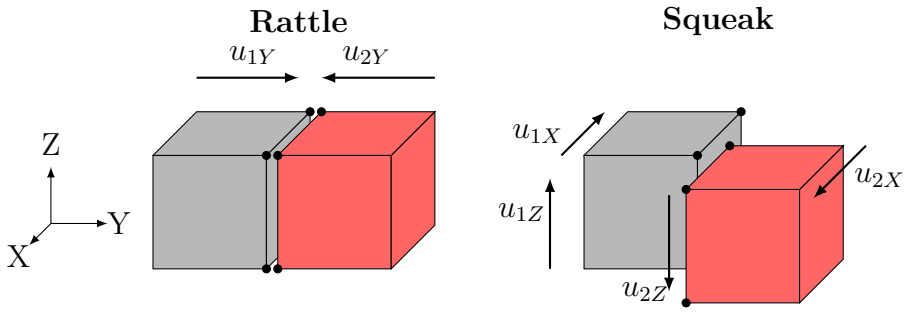

Figure 1.1: *Two adjacent parts separated by colour. Rattle phenomena is visualised to the left and squeak phenomena is visualised to the right.*

is currently a gap of guidelines as the research within the area is still at an early stage, and no standard method has emerged [3].

The most common FE (finite element) packages, such as NASTRAN & ABAQUS, support dynamic substructuring for linear systems based on the Craig-Bampton method [4] & [5]. Nonlinear analyses are computational heavier than linear analyses. Hence, it would be beneficial if the CMS method is applicable for S&R-simulations including nonlinearities in the form of contact. It has earlier showed good potential for systems with weak nonlinear effects. However, as the nonlinear effects increase, the accuracy decreases due to the approximations of the linear reduction techniques [6].

The model which will be used in this thesis, for analysis of substructures in nonlinear S&R simulation, is schematically visualised in Figure 1.2. The model is the front door of a passenger car, and it is suggested by VCC as the contact between the inner panel and the structural frame is listed under critical sections for demonstrating S&R. The figure schematically shows the principle of the CMS method. The full model can be seen to the left where the inner panel and the structural frame are separated by colour. The grey part represents the structural frame and the red part represents the inner panel. The gap between these two will, in case of S&R, open and close in non-stationary manner, due to the relative movement of the adjacent parts. In case of contact, nonlinearities will appear in the model. However, by assuming linearity, the CMS method can be used to reduce the number of DOFs. The right figure shows a schematic figure of the assembled substructured system, with a lower number of DOFs in the area where linearity is assumed.

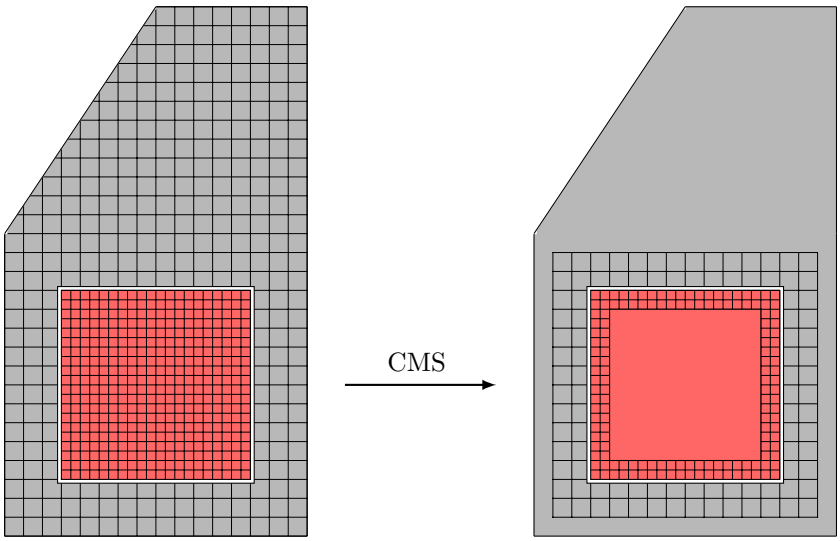

Figure 1.2: *Schematic figure of the inside of a car door with two adjacent parts. Full model to the left and model with reduced number of DOFs to the right.*

1.2 Objective

The purpose of this thesis work, which is a part of a larger doctoral project, is to evaluate how the CMS method of Craig-Bampton can be used in systems including nonlinearities in the form of contact. This aims to improve VCC's CAE process by creating modelling guidelines for how to implement the CMS method in analyses including nonlinearities in the form of contact. The aim is to try out different substructure configurations and to write guidelines on how to use the method in nonlinear S&R simulations.

The thesis work will give answer to the following questions:

- Is it possible to use the Craig-Bampton method for S&R simulations including nonlinearities without sacrificing the accuracy of S&R prediction in design phase?
- How sensitive, with respect to S&R, is the area around the interface?
- How close to the interface can DOFs be removed without affecting the accuracy of the results?
- Is it possible to increase the efficiency of the simulation by adjusting the model reduction approach for the specific application?
- What is the correlation between computational cost, number of DOFs and accuracy?

The results from the substructured FE-model will be compared to the results from a full FE-model by means of eigenvector comparison, frequency response comparison and by comparing contact event with respect to time and amplitude.

1.3 Limitations

The meshed FE-model is provided by VCC and a mesh convergence study of the whole model is out of scope. Linear isotropic elastic material properties are assumed, and no plastic deformation will be considered. This is an assumption as materials generally are anisotropic and nonlinear in reality. The assumption is based on the fact that the problem on hand deals with loads far below the yield limit.

Due to the time constraint of this thesis work, the FE-model will not be validated with experimental results from testing. For verification of the reduced model, the full model will be used as a reference.

Due to computational limitations, frequencies above 1000 Hz will not be considered during the FE-analyses, with an exception for the generation of substructures. Also, the maximum number of periods of the excitation signal is considered to be five. This is based on an assumption about a periodic response after four periods.

2

Theory

In this chapter, the theory used during the thesis work is presented. First, an introduction to modal analysis and how to convert a time domain signal into frequency domain using the Fourier transform is given. Next, an introduction to dynamic substructuring and the CMS method, is revised. Then, the excitation signal generation and the verification process is explained. Finally, some basic FEM solver settings used in this thesis are discussed.

2.1 Modal analysis

Modal analysis is used to obtain natural frequencies and mode shapes of a system. Consider the undamped dynamical system below

$$\boldsymbol{M}\ddot{\boldsymbol{q}} + \boldsymbol{K}\boldsymbol{q} = \boldsymbol{0} \tag{2.1}$$

where $\boldsymbol{M}$ is the mass matrix and $\boldsymbol{K}$ is the stiffness matrix. The mathematical representation of the eigenvalue problem for this system reads as follows:

$$(\boldsymbol{K} - \omega^2 \boldsymbol{M})\boldsymbol{x} = \boldsymbol{0} \tag{2.2}$$

where ω corresponds to the angular frequency of the system and $\boldsymbol{x}$ corresponds to the eigenvectors.

Material properties and boundary conditions affect the modal behaviour of a system. When material properties or boundary conditions of a structure changes, its modal behaviour also changes [7]. Thus, modal analysis can provide useful information about the dynamic behaviour of a system.

2.2 Fourier transform

The method for transforming a function of time into a function of frequency is called Fourier transform [8]. Inverse Fourier transform is used to convert information from frequency domain to time domain. The Fourier transform can be represented mathematically according to:

$$Y(\omega) = \int_{-\infty}^{\infty} y(t)\, e^{-j\omega t} dt \tag{2.3}$$

The inverse Fourier transform can be mathematically represented as:

$$y\left(t\right)=\int_{-\infty}^{\infty}Y\left(\omega\right)e^{-j\omega t}d\omega \tag{2.4}$$

where ω is the angular frequency and t is the time. Here, y represents the signal in time domain and Y represents the signal in frequency domain.

Fast Fourier transform (FFT) is the name of a fast algorithm that computes the discrete Fourier transform. Inverse fast Fourier transform (IFFT) is the name of a fast algorithm that converts the information from frequency domain to time domain [9]. The transformations are performed according to:

$$Y(\omega)=\sum_{t=1}^{n}y(t)W_{n}^{(t-1)(\omega-1)} \tag{2.5}$$

$$y(t)=\frac{1}{n}\sum_{\omega=1}^{n}Y(\omega)W_{n}^{-(t-1)(\omega-1)} \tag{2.6}$$

where $W_n=e^{(-2\pi i)/n}$ and n is the length of $y(t)$ and $Y(\omega)$ [10].

2.3 Transfer function

The principle of a transfer function in frequency domain is shown in Figure 2.1. The function consists of a real- and an imaginary part, and can therefore be expressed as magnitude and phase [11]. The relation of the input force and the response of the structure can in frequency domain be express as:

$$R(f)=H(f)F(f) \tag{2.7}$$

where it is assumed that the system is linear. The response of the mechanical system, $R(f)$, can be any kinetic response parameter of the structure, such as displacement, velocity or acceleration. Transfer functions can be used to identify nonlinear responses of a system [12], as the function, in case of linearity, should be the same independent of scaling of the stimulus. The output *R(f)* in this thesis is referred to as the frequency response.

2.4 Dynamic substructuring

Dynamic substructuring is an approach where a structural system is analysed separately by decomposing it into several simple components [3]. The method is based on finding the dynamic behaviour of the entire system by assembling the dynamic

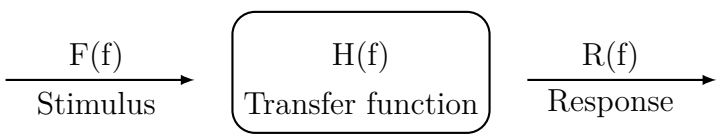

Figure 2.1: *Visualisation of a transfer function. F(f) is the stimulus, H(f) is the transfer function and R(f) is the structural response.*

behaviour of its different components (substructures) [13]. Much research has been carried out in the field of dynamic substructuring [3], whereby different methods have emerged.

2.4.1 Component Mode Synthesis

Well known methods of dynamic substructuring are the ones classified as CMS. The method combines the idea of decomposing a system into substructures, analysing these separately and then assemble it again with techniques of model reduction. One of the most popular CMS-method is the Craig-Bampton method [14], which reduces the number of DOFs using fixed interface vibration modes and static condensation modes (Guyan modes) [15].

2.4.1.1 Guyan modes

By considering the Guyan modes it is possible to remove all internal DOFs of a substructure and retain only the interface DOFs connecting the substructure to the rest of the model. The Guyan mode matrix is based on the response associated to a unit displacement to each interface DOF, while the rest of the interface DOFs are constrained [4]. Consider the undamped dynamical system below:

$$\boldsymbol{M}\ddot{\boldsymbol{q}} + \boldsymbol{K}\boldsymbol{q} = \boldsymbol{F} \tag{2.8}$$

Partitioning Equation 2.8 into internal DOFs, $\boldsymbol{q}_i$, and boundary DOFs, $\boldsymbol{q}_b$, gives

$$\begin{bmatrix} \boldsymbol{M_{bb}} & \boldsymbol{M_{bi}} \\ \boldsymbol{M_{bi}} & \boldsymbol{M_{ii}} \end{bmatrix} \begin{bmatrix} \ddot{\boldsymbol{q}}_b \\ \ddot{\boldsymbol{q}}_i \end{bmatrix} + \begin{bmatrix} \boldsymbol{K_{bb}} & \boldsymbol{K_{bi}} \\ \boldsymbol{K_{bi}} & \boldsymbol{K_{ii}} \end{bmatrix} \begin{bmatrix} \boldsymbol{q}_b \\ \boldsymbol{q}_i \end{bmatrix} = \begin{bmatrix} \boldsymbol{F}_b \\ \boldsymbol{F}_i \end{bmatrix} \tag{2.9}$$

Consider the second row of Equation system 2.9 and assume that no internal force is applied to the internal DOFs according to

$$\boldsymbol{M}_{bi}\ddot{\boldsymbol{q}}_b + \boldsymbol{M}_{ii}\ddot{\boldsymbol{q}}_i + \boldsymbol{K}_{bi}\boldsymbol{q}_b + \boldsymbol{K}_{ii}\boldsymbol{q}_i = \boldsymbol{0} \tag{2.10}$$

Since the Guyan modes are based on the static response, the inertia effects can be neglected which leaves:

$$\boldsymbol{K}_{bi}\boldsymbol{q}_b + \boldsymbol{K}_{ii}\boldsymbol{q}_i = \boldsymbol{0} \tag{2.11}$$

which in turn gives:

$$\boldsymbol{q}_i = -\boldsymbol{K}_{ii}^{-1}\boldsymbol{K}_{bi}\boldsymbol{q}_b \tag{2.12}$$

where $-\boldsymbol{K}_{ii}^{-1}\boldsymbol{K}_{bi}$ are the static modes. By considering the original DOF-set, we can express all DOFs in terms of boundary DOFs according to:

$$\boldsymbol{q} = \begin{bmatrix} \boldsymbol{q}_b \\ \boldsymbol{q}_i \end{bmatrix} = \begin{bmatrix} \boldsymbol{I} \\ -\boldsymbol{K}_{ii}^{-1}\boldsymbol{K}_{bi} \end{bmatrix} \boldsymbol{q}_b = \begin{bmatrix} \boldsymbol{I} \\ \boldsymbol{\Psi}_c \end{bmatrix} \boldsymbol{q}_b \tag{2.13}$$

2.4.1.2 Fixed interface vibration modes

Considering the fixed interface vibration modes makes it possible to also include the dynamic behaviour of the structure in the substructured system. This is done by reducing the number of internal DOFs to a decreased number of so called generalised DOFs.

Consider once again the undamped dynamical system in Equation 2.8. When calculating the fixed interface vibration modes, the system is once again partitioned into internal DOFs, $\boldsymbol{q}_i$ and boundary DOFs, $\boldsymbol{q}_b$ as in Equation 2.9. As the name of the fixed interface vibration modes imply, the boundary DOFs in Equation 2.9 are constrained ($\boldsymbol{q}_b = \boldsymbol{0}$). Consider now the second row of the equation system.

$$\boldsymbol{M}_{ii}\ddot{\boldsymbol{q}}_i + \boldsymbol{K}_{ii}\boldsymbol{q}_i = \boldsymbol{0} \tag{2.14}$$

Solving the eigenvalues of equation system 2.14 gives the fixed interface vibration modes according to

$$[\boldsymbol{K}_{ii} - \omega_j^2 \boldsymbol{M}_{ii}]\{\boldsymbol{\alpha_i}\}_j = \boldsymbol{0} \tag{2.15}$$

where $\boldsymbol{\alpha}$ is the solution to Equation 2.15. Assembling the eigenvectors gives the matrix of fixed interface vibration modes, $\boldsymbol{\Phi}_i$ [16].

2.4.1.3 Craig-Bampton reduction matrix

The reduction matrix of Craig-Bampton, $\boldsymbol{\Psi}_{CB}$, consists of a combination of the Guyan modes and the fixed interface vibration modes. By describing the system in terms of the Guyan modes, $\boldsymbol{\Psi}_c$, and the fixed interface vibration modes $\boldsymbol{\Phi}_i$ we get

$$\begin{bmatrix} \boldsymbol{q}_b \\ \boldsymbol{q}_i \end{bmatrix} = \boldsymbol{\Psi}_{CB} \begin{bmatrix} \boldsymbol{q}_b \\ \boldsymbol{\eta} \end{bmatrix} \tag{2.16}$$

where $\boldsymbol{\eta}$ is a vector containing the generalised DOFs. From section 2.4.1.1 and 2.4.1.2 we can identify the Craig-Bampton reduction matrix as

$$\boldsymbol{\Psi}_{CB} = \begin{bmatrix} \boldsymbol{I} & \boldsymbol{0} \\ \boldsymbol{\Psi}_c & \boldsymbol{\Phi}_i \end{bmatrix} \tag{2.17}$$

Consider once again Equation 2.8, which now by using the Craig Bampton matrix can be re reformulated to:

$$[\boldsymbol{\Psi}_{CB}^T \boldsymbol{M} \boldsymbol{\Psi}_{CB}] \begin{Bmatrix} \ddot{\boldsymbol{q}}_b \\ \ddot{\boldsymbol{\eta}} \end{Bmatrix} + [\boldsymbol{\Psi}_{CB}^T \boldsymbol{K} \boldsymbol{\Psi}_{CB}] \begin{Bmatrix} \boldsymbol{q}_b \\ \boldsymbol{\eta} \end{Bmatrix} = \boldsymbol{\Psi}_{CB}^T \boldsymbol{F} \tag{2.18}$$

which can be written as

$$\boldsymbol{M}_{CB} \begin{Bmatrix} \ddot{\boldsymbol{q}}_b \\ \ddot{\boldsymbol{\eta}} \end{Bmatrix} + \boldsymbol{K}_{CB} \begin{Bmatrix} \boldsymbol{q}_b \\ \boldsymbol{\eta} \end{Bmatrix} = \boldsymbol{F}_{CB} \tag{2.19}$$

where

$$\boldsymbol{M}_{CB} = \boldsymbol{\Psi}_{CB}^T \boldsymbol{M} \boldsymbol{\Psi}_{CB}$$
$$\boldsymbol{K}_{CB} = \boldsymbol{\Psi}_{CB}^T \boldsymbol{K} \boldsymbol{\Psi}_{CB}$$
$$\boldsymbol{F}_{CB} = \boldsymbol{\Psi}_{CB}^T \boldsymbol{F}$$

2.5 Random phase multi-sine

In order to get information about a systems dynamic behaviour over a given frequency range, there are several different stimulus types that are suitable [12]. This includes a random phase multi-sine signal. The signal is constructed by combining harmonic sine waves with a constant amplitude and a phase angle randomly selected from normal distributed range between 0 and 2π. All information obtained from a stepped sine test can be obtained by using a random phase multisine, but with a lower computational cost [12]. The perks of using a random phase multi-sine includes the possibility of controlling the frequency and the amplitude spectrum [17]. The signal is created in the frequency domain and is realised in time domain by using IFFT.

The random phase multi sine is expressed as [12]:

$$u(t) = Re\left\{ \sum_{n=-N}^{N} U_k \cdot e^{i(2\pi k f_0 t + \phi_k)} \right\}, \;\; k \neq 0 \tag{2.20}$$

where N is the total number of sine waves, f_0 is the fundamental excitation frequencies, ϕ_k are the randomly selected phases obtained from a normal distributed range of $[0, 2\pi]$ and U_k is the amplitude [12].

2.6 Model verification

As the model is reduced using the CMS method, it is important make sure that it is a good representation of the original system. This is done by verifying the model which is described here.

2.6.1 Modal Assurance Criterion

The Modal Assurance Criterion (MAC) compares two models by means of eigenvector comparison [18]. It is often used to compare CAE results with experimental results [18], but might as well be used to compare a substructured model with a full model. Let us call the eigenvectors obtained from the full model as $\boldsymbol{v}^{(k)F}$ and the eigenvectors from the substructured model as $\boldsymbol{v}^{(k)R}$. These are determined by shape, and are therefore independent of scaling factor. MAC is based on the angle between the eigenvectors. If the two sets are identical, this angle is zero. Taking the squared cosine value of the angle gives the MAC value according to [18]:

$$MAC(i,j) = \frac{((\boldsymbol{v}^{(i)R})^T \boldsymbol{v}^{(j)F})^2}{(|\boldsymbol{v}^{(i)R}||\boldsymbol{v}^{(j)F}|)^2} \tag{2.21}$$

If the eigenvectors are co-linear, the MAC value is one, and if they are orthogonal, it is zero. For partially co-linear mode pairs, the MAC value is $0 < MAC < 1$.

2.6.2 Verification including nonlinearities

MAC can only be used to compare the modal behaviour. To include nonlinear effects in the comparison, the frequency response functions can be compared. In order to verify the nonlinear system response accurately, one step of the verification process is to make sure that it does not contain a significant amount of transients [12]. A periodic input load should generate a periodic response once the transients have faded out.

The frequency response functions can be compared using normalised root mean square error [10] according to:

$$NRMSE = 1 - \frac{||d_r(:,i) - d(:,i)||}{||d_r(:,i) - d_{r,m}(:,i)||} \tag{2.22}$$

where d_r is the reference data set, $d_{r,m}$ is the mean value of the reference data set, d is the data to be compared and $||\cdot||$ symbolises the 2-norm of a data set [10].

The value of NRMSE varies between -Inf (represents a bad fit) to 1 (represents a perfect fit). A value of 0 indicates that the vector compared does not give a better fit than a straight line would [10].

2.7 Omega arithmetic

Accelerometers are often used to measure acceleration on moving vehicles [19]. Velocity and displacement is then obtained by integrating the acceleration. However, when performing the integration, the low-frequency content can easily result in wrong interpretations of the velocity and displacement, resulting in a drift of the integrated acceleration [19]. Omega arithmetic is used to remove the drift by converting the acceleration signal into the frequency domain, filter away the low-frequency content and then convert it back into the time domain. The benefits of using Omega Arithmetic is that it allows you to remove the drift without losing important information about the data. FFT and IFFT concepts described in section 2.2 are used to transform the signal between time and frequency domain. For a more detailed explanation about the method, see reference [19].

2.8 Linear and nonlinear FEM

The finite element method (FEM) is a numerical approach used to obtain solutions to structural engineering problems including differential equations, given a set of boundary conditions [20]. The characteristics of a finite element is highly dependent of the element stiffness matrix. The element stiffness matrix describes the material and the geometrical features of the element. Equation 2.23 describes the basics of static FEM.

$$\boldsymbol{K} \cdot \boldsymbol{q} = \boldsymbol{F} \tag{2.23}$$

$\boldsymbol{K}$ is the element stiffness matrix, $\boldsymbol{q}$ is the nodal displacement vector, and $\boldsymbol{F}$ is the nodal load vector.

The stiffness matrix is the central difference between a linear and a nonlinear analysis. When an element deforms, the stiffness matrix changes which can affect critical aspects of the structure. A linear FE-analysis assumes that the change of the element stiffness matrices are negligible [21]. This means that for a linear analysis, the stiffness matrix stays the same through out the whole analysis, regardless the extension of the deformation or load. In linear analysis, $\boldsymbol{K}$ only needs to be solved and assembled once which means that there is no need of updating it during the analysis.

In a nonlinear FE-analysis on the other hand, we leave the assumption about a negligible change of the stiffness matrix [21]. Instead, it varies during the analysis, as it depends on the deformation and the loading of the structure. In a nonlinear analysis, $\boldsymbol{K}$ needs to be solved and updated in an iterative process at every time step, which increases the simulation costs significantly [21].

A nonlinear behaviour can be the affect of several different phenomena which include large displacements, nonlinear material and contact. The latter is the one causing nonlinearities in this study, which is a result of adjacent parts impacting to each other.

2.9 Implicit- and explicit solvers in FEA

Implicit and explicit solvers are the iterative methods used in FEA (Finite Element Analysis). The type of the specific analysis along with the desired level of accuracy usually decides the solver. In automotive industry, the explicit solver is often used for crash analyses while the implicit solver is used to solve static or "smooth" nonlinear problems [22].

In implicit solvers, the equations are coupled and solved simultaneously. The implicit solvers are unconditionally stable for linear problems, and it considers large time steps to attain faster convergence. However small iterative steps are used to achieve convergence for nonlinear problems. On the other hand in explicit solvers, the equations are uncoupled and solved explicitly. It is only stable if the size of each time step is smaller than the critical time step which is dependent of the wave propagation and the element size.

Implicit solvers can be used for object impacts below 6.71 m/s [23]. Rattle events generally have an impact velocity below this [24], which means that the implicit solver can be used for this study. In Abaqus, Abaqus/Standard option is selected for implicit analysis where as ABAQUS/Explicit option is selected for explicit analysis[22].

2.10 Penalty method

Penalty method assumes that the contact force is proportional to the contact gap. The method tries to prevent penetration between contact surface by assuming a very large force associated to it [26]. The contact energy equation is shown below.

$$\pi_c = \frac{1}{2}\kappa \cdot g_N^2 \tag{2.24}$$

where π_c is the contact energy function, g_N is the current normal gap between contact surfaces and κ is a large number.

Equation 2.24 is similar to the spring energy equation. The equation can be explained as during contact it assumes large stiffness values in order to prevent contact penetration. However, the method results in some amount of penetration unless κ value approaches infinity. For a node in contact, the method modifies the stiffness matrix and force vector. Assume m and n are DOFs associated to a node in contact. The stiffness matrix and force vector corresponding to m and n dofs are modified as shown below.

$$\overline{K} = \begin{pmatrix} K_{11} & K_{12} & ... & K_{1m} & ... & K_{1n} & ... & K_{NN} \\ K_{21} & ... & ... & ... & ... & .... & ... & K_{2N} \\ ... & ... & ... & ... & ... & .... & ... & ... \\ K_{m1} & K_{m2} & ... & K_{mm} + \kappa \hat{n_1}^1 \cdot \hat{n_1}^1 & ... & K_{mn} + \kappa \hat{n_1}^1 \cdot \hat{n_2}^1 & ... & K_{mN} \\ ... & ... & ... & ... & ... & .... & ... & ... \\ K_{n1} & K_{n2} & ... & K_{nm} + \kappa \hat{n_2}^1 \cdot \hat{n_1}^1 & ... & K_{nn} + \kappa \hat{n_2}^1 \cdot \hat{n_2}^1 & ... & K_{nN} \\ ... & ... & ... & ... & ... & .... & ... & ... \\ K_{N1} & ... & ... & ... & ... & .... & ... & K_{NN} \end{pmatrix}$$

$$\overline{F} = \begin{bmatrix} F1 \\ F2 \\ ... \\ F_m - \kappa \cdot G_N \cdot \hat{n_1}^1 \\ ... \\ F_n - \kappa \cdot G_N \cdot \hat{n_2}^1 \\ ... \\ F_{NN} \end{bmatrix}$$

where G_N is initial normal gap, $\hat{n^1}$ is the unit normal [27].

2.11 Contact definition

For FE-problems including contact, a contact definition is required. In this thesis, the possible sets of contact nodes are found from the contact definition using penalty method. The penetration of the possible contact nodes are checked. The stiffness matrix and the force vector of the nodes that are in contact are modified according to Section 2.10.

In the automotive industry, the contact is often defined using shell elements as they are computationally more efficient than solid elements. Shell elements have double-sided surfaces. ABAQUS offers two types of contact definitions. One is surface to surface (StS) and the other one is node to surface (NtS) contact definition. In StS contact definition, master and slave surfaces are defined as element based surfaces. This type of definition can work with double sided surfaces. In NtS contact definition, master surface should again be defined as an element based surface whereas slave surface is defined as node based surface. This type of definition cannot work with double sided surfaces [4]. Comparison of these two contact definition is referred from [28]. The main arguments are summarised as follows: StS contact definition reduces the possibility of penetration between master and slave surface. It is also less sensitive to the choice of master and slave surface. More nodes per constraints tends to be involved in StS when compared to NtS based contact formulation, so it is numerically more stable.

3
Method

This chapter presents the method used to evaluate how the CMS method of Craig-Bampton can be used in nonlinear S&R simulations. First, an introduction to the model is given and an explanation of how it is simplified. Next, the excitation signal generation is explained, based on previous experimental results. Then, the substructure generation and a study of number of retained DOFs is revised. Finally, the verification procedure is explained.

3.1 Model

As mentioned in the introduction, the study is carried out on a car door where the critical area for S&R issues is identified as the interface between the inner panel and the structural frame.

3.1.1 Previous study of model

In a previous physical experimental study [24], the door was mounted to a fixture which was excited using recorded road load data from Pave, which is a road track well known for generating S&R issues. The excitation signal had a mean of zero and a frequency content below 100 Hz. The setup used during the physical experiment set up can be seen in Appendix A, Figure A.1, where the green, blue and red boxes represent regions of the mounting interfaces to the fixture. In addition, the blue and the green boxes represent locations where sensors were placed. The sensors measured acceleration. The sensor on the front side (green box) measured in X-, Y- and Z-direction and the sensor on the rear side (blue box) measured in Y- and Z-direction.

To get information on how to create the excitation signal, which will be applied to the FE-model, the experimental data is post-processed and analysed in MATLAB. As it is easier to identify noises and disturbances in displacement data, the acceleration is integrated twice. However, this shows a drift in the displacement data, which significantly moves the mean away from zero, due to noises in the system and also because of accumulated errors of the numerical integration. The drift is visualised in Figure 3.1.

To remove this drift, Mercer showed in his paper [19], that the Omega Arithmetic method can be used. By trying different frequency values, it was concluded that with all content below 7 Hz filtered away, the integrated signal has a zero mean, which

can be seen in Figure 3.2. The maximum amplitude of the 62 second long signal is identified as 1.9 mm. Based on a sampling frequency of 48 kHz, the frequency content of the recorded signals showed to be located below 100 Hz, which can be seen in Figure 3.3.

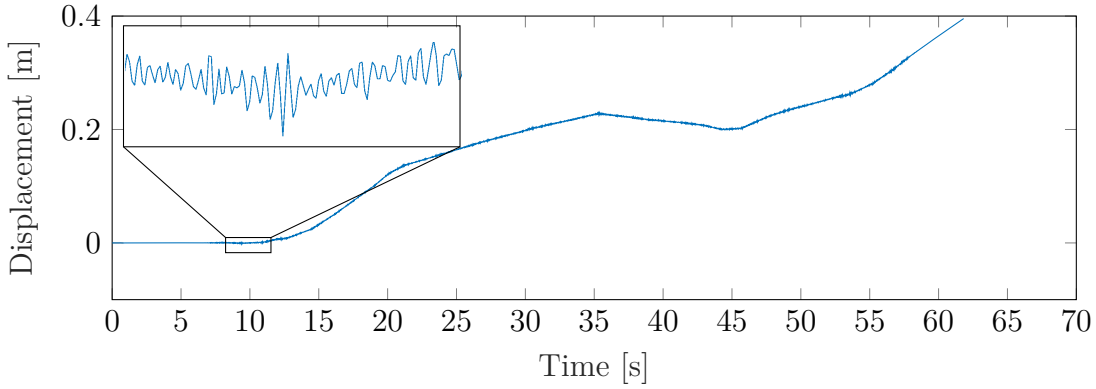

Figure 3.1: *Z-directional displacement in the front hinge of the car door obtained by integrating the measured acceleration data twice.*

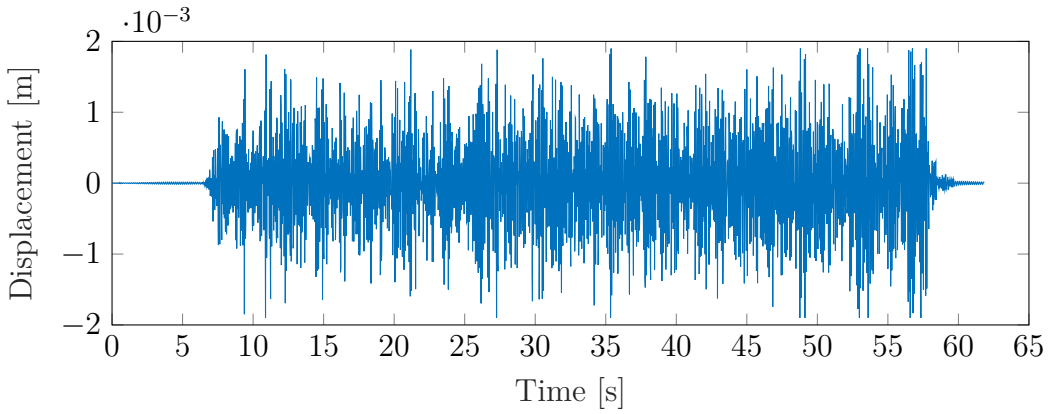

Figure 3.2: *Z-directional displacement in the front hinge after it is filtered using the Omega Arithmetic's method.*

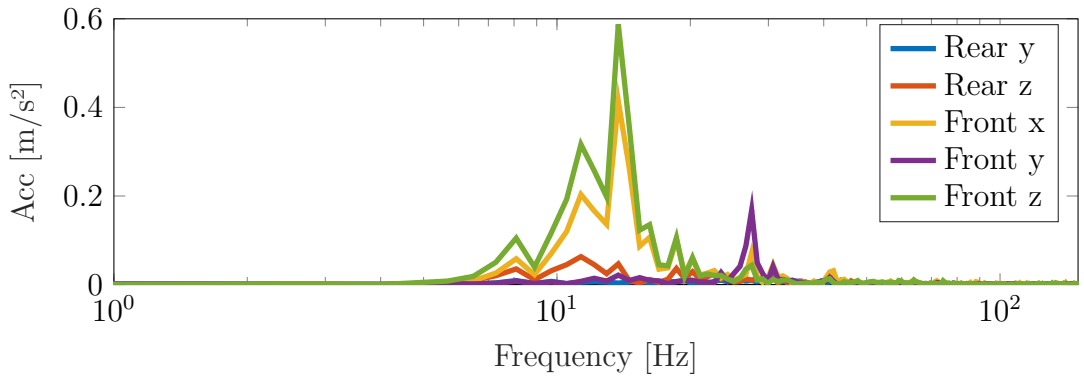

Figure 3.3: *Frequency content of recorded acceleration signals.*

Table 3.1: *Details about the FE-model. E is Young's modulus, ν is Poisson's ratio and ρ is density.*

Part	E [GPa]	ν [-]	ρ $[kg/m^3]$	Element type	Thickness [mm]
Frame	210.00	0.3	7 850	Shell elements	0.7
Carrier	4.05	0.4	1 120	Shell elements	1.8
Panel	3.50	0.25	830	Shell elements	1.8

Table 3.2: *Comparison between original model and simplified model.*

	Full model	Simplified model
Mass [kg]	28.11	10.05
# DOFs	2 589 830	1 169 406

3.1.2 FE-model

The FE-model has a high level of modelling details and contains several sources of nonlinearities. Since this thesis aims to increase the understanding of how to use substructures in nonlinear simulations including contact, the complex model is simplified.

3.1.2.1 Simplification of FE-model

Due to the size and complexity of the FE-model, it is reduced to the three main parts shown in Figure 3.4. The simplified model consists of the frame[1], the carrier[2] and the inner panel[3]. Details about each part can be seen in Table 3.1. The inner panel is connected to the frame through two hooks and one screw. It is also connected with six hooks to the carrier which in turn is connected with 13 screws to the frame. Table 3.2 shows the mass and the number of DOFs for the original and the simplified model. The global coordinate system is shown in Figure 3.5. Y-direction corresponds to the normal direction (rattle direction) between the frame and the panel and the initial gap between the parts is 3.7 mm.

All forms of nonlinearities, except for contact, is removed. The material model provided by VCC has plastic- and creep properties. It is reconstructed with linear material properties. Another form of nonlinearity comes from the links in the hooks, which are used to connect the panel to the rest of the model. The links allow small defined translations in specified directions. After the defined value, the links act in a rigid way. These links are replaced with rigid links, which gives a constant linear behaviour in the connection points.

After simplification, the only nonlinearity is coming from the contact between the frame and the inner panel. The contact region, which is highlighted in Figure 3.5, is defined by VCC. The red marked region represents the surface of the panel for which contact is defined, and the blue marked region represents the contact surface for the frame. The contact definition is based on StS contact, which is defined for 2D shell elements. The zoomed in region in Figure 3.5 shows parts of the contact

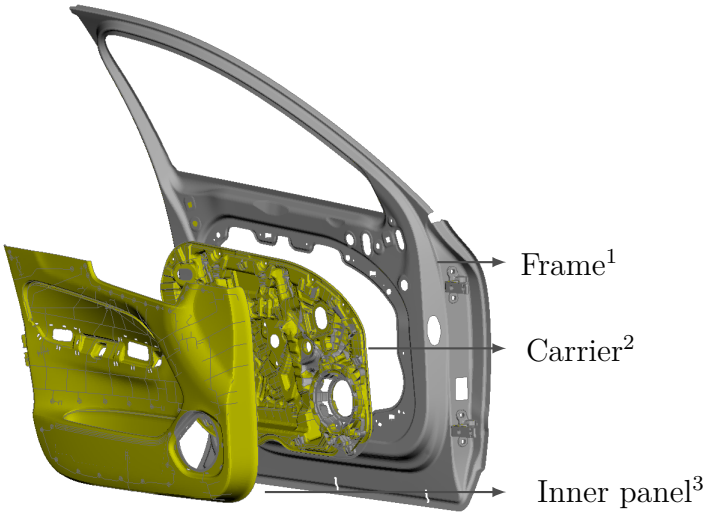

Figure 3.4: *Three main components of the simplified car door.*

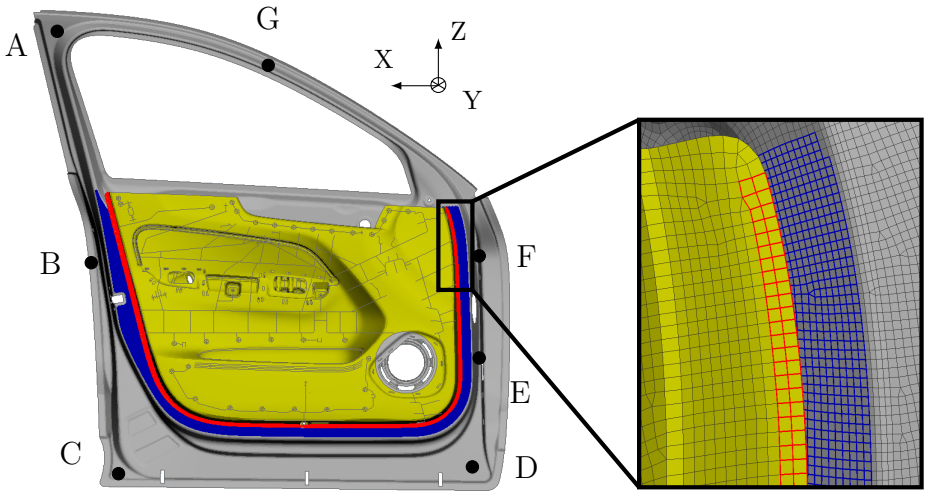

Figure 3.5: *FE-model - Points where boundary conditions are applied are marked in black and contact surfaces are highlighted in red and blue.*

surface, where it can be seen that contact for the panel is defined for two rows of elements on the edge of the panel. The contact surface for the frame is defined for a larger area, in order to capture all potential contact events.

3.1.2.2 Boundary conditions

The FE-model is analysed with conditions similar to those present during the physical experiment of the model. Table 3.3, together with Figure 3.5, shows the boundary conditions. The load is applied as enforced displacement in Z-direction on the upper hinge location on the front side of the car door. It is scaled in 4 different ways which is described more detailed in Section 3.2.

Table 3.3: *Boundary conditions for the FE-model, where ⋆ denotes constrained and ◇ denotes load applied as enforced displacement.*

Point	X	Y	Z	RX	RY	RZ
A		⋆				
B	⋆	⋆	⋆	⋆	⋆	⋆
C		⋆				⋆
D		⋆				⋆
E		⋆				
F		⋆	◇			
G		⋆				

Table 3.4: *The different amplitudes with corresponding notation, number of contact events per second and the amplitude of the sine-waves.*

Notation	Contact events per second	Amplitude [mm]
A1	0	0.001
A2	4-6	1.4
A3	8-12	1.6
A4 (Reference load)	13-17	1.9

3.2 Excitation signal

Since the recorded signal is 62 second long, it is too computationally heavy to use as an excitation signal in the FE-analysis, due to the computational limits of this thesis. Therefore, a random phase multisine signal is constructed based on the content of the experimentally recorded data. This allows for all frequencies of interest to be excited with the same amplitude during a specified time range. Based on the frequency content and the maximum displacement of the recorded data, the frequency range of the signal is set to 0-100 Hz and the amplitude of the sine-waves for the reference load is set to 1.9 mm. The reference load is used to check the behaviour of the model and to identify critical areas for contact.

Generally, for S&R issues, around 5-15 contact events occur during a second [25]. To cover this range and to make the study more general, the excitation signal is scaled in four different levels. This is to generate three different levels of contact. One load is also scaled in such way that no contact occur. This load is used to see how accurate the reduced model is under linear, dynamic, conditions. The four loads, with corresponding notation, can be seen in Table 3.4.

The excitation signal is repeated in a periodic way, where each period is one second long. Since the most important part of this study is to compare the reduced model to the reference model, it is assumed that after four periods, the system response is periodic. This assumption is based on the fact that the comparison between the two models is more important than the dynamic behaviour of the system. Therefore, potential transients after four periods should be the same for the reduced and the

reference model, if they are well correlated.

3.2.1 Sampling frequency and time steps

Based on the Nyquist theorem [29], the sampling frequency should be at least 200 Hz, since the maximum frequency of the excitation signal is 100 Hz. The analysis includes nonlinearities though, which means that additional multiples should be considered. Using a multiple of 5 to account for nonlinearities, the sampling frequency is set to 1000 Hz, which is 10 times higher than the frequency of the excitation signal.

Rattle events are generally not shorter than 5 milliseconds [30]. By using time steps of 1 millisecond, contact events within a time span of one millisecond can be captured. Considering smaller time steps is computationally too expensive and is considered as a limitation of the work reported in this thesis.

3.3 Dynamic substructuring

The three components in Figure 3.4 are treated as substructures and are reduced using the Craig-Bampton method. The three components are connected to each other through the hooks and screws described in Section 3.1.2. The nodes to which the rigid links are connected are defined as master nodes of Multi-Point Constraints (MPCs), which distribute the force to a number of selected nodes around the connection points. When generating the substructures, all these master nodes are defined as retained nodes in order to properly connect the substructures to each other.

ABAQUS doesn't allow for the user to define surface definitions on a substructure. When generating the substructures, the surfaces on which contact is defined therefore need to be taken into account. For the frame and the inner panel, according to Figure 3.5, a large portion of DOFs has to be added in order to connect the contact regions to the rest of the model. Figure 3.6 visualises the phenomena of using substructures when surface based contact definitions are present. As can be seen, the number of retained nodes is high in relation to the number of nodes in the full model.

The substructured model in this study is referred to as the reduced model. The original model, which is not decomposed, is referred to as the reference model or

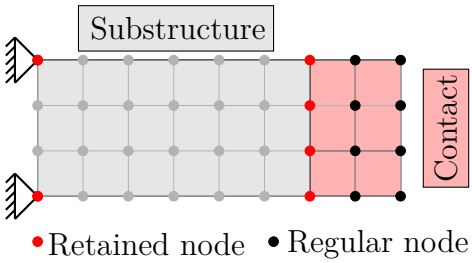

Figure 3.6: *Schematic figure of the principle of using substructures when contact definitions are present.*

"ref" which is the notation in figures and tables. In tables and figures rDOFs is the notation for "retained DOFs".

3.3.1 Relation between retained DOFs and CPU-time

The purpose of using substructures is to improve the computational efficiency. In ABAQUS, however, the method can have the opposite effect if the number of retained DOFs is too high. The drawback is based on the fact that the reduced stiffness- and mass matrices of the substructures are fully populated. This can in turn affect the wave-front of model which can have a negative effect in the computational cost [4].

Based on this fact, the relation between the number of retained DOFs and computational time is evaluated. Since the frame carries the largest contact area, and therefore the highest number of retained DOFs, the study is performed by changing the number of retained DOFs along the contact interface for the frame. This corresponds to all nodes along the blue line in Figure 3.7(a). During this study only the carrier and the frame are substructured with panel included in the unsubstructured model.

Table 3.5 shows the different configurations that are analysed, where C1 represents the case when all interface DOFs of the frame are retained. The number of retained DOFs is then gradually decreased until the stage where no significant change can be seen in CPU-time. When decreasing the number of retained DOFs, these are distributed equally along the interface. It means that some nodes of the substructure are free and not coupled to the rest of the model. To see the accuracy of the substructured model, a set of 15 verification node pairs are selected along the contact region. Each pair consisting of one node located on the frame and one on the panel. The locations of the node pairs can be seen in Figure 3.7(b). The eigenvalue problem is solved for frequencies up to 100 Hz. The reduced model is then compared to the reference model based on the eigenvectors.

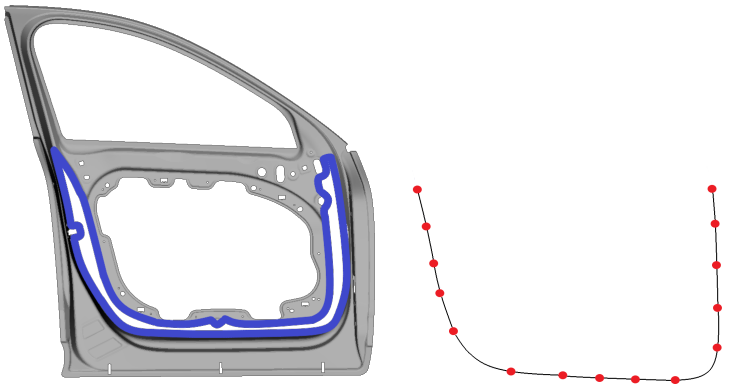

(a) *Frame contact interface.* **(b)** *Verification nodes during run time study.*

Figure 3.7: *Frame contact interface. The blue line represents the interface between the contact surface and the frame substructure. The verification node pairs are shown in red.*

Table 3.5: *Influence of number of retained DOFs with respect to CPU-time.*

Notation	Node space[A]	# rDOFs[B]	CPU-time[C] [$\cdot 10^3$ s]
Ref	-	-	39.44
C1	1	8 280	49.17
C2	2	4 146	20.39
C3	4	2 076	14.94
C4	8	1 032	14.57
C5	16	516	13.39

[A] A value of x means that every xth node along the blue line in Figure 3.7(a) is retained.
[B] Number of retained DOFs for the frame substructure.
[C] Based on a nonlinear dynamic analysis.

The resulting CPU-times, also seen in Table 3.5, show that when keeping all the interface DOFs for the frame substructure, the CPU-time actually increases in comparison to the reference model. As the study proceeds, it is concluded that the CPU-time stagnates at the point where 1000-2000 DOFs are retained for the frame substructure. This however, decreases the accuracy of S&R prediction, as the substructure is not fully connected to the rest of the model. Figure 3.8 shows the MAC-correlation between the reduced models and the reference model. C1, which has the best correlation can be seen to the left in the figure. C5, which has the worst can be seen to the right in the figure. As can be seen for C1, the entire diagonal carries values close to one. For C5 though, only 8-12 mode shapes are captured accurately.

Figure 3.9 shows the diagonal values of the MAC-matrix for all configurations. As expected, the MAC-values of the diagonal gradually decreases from C1 to C5. For C2, lower MAC values can be seen for 8-10 modes. To find a balance between accuracy and computational time, the entire contact region can therefore not be analysed with all interface DOFs retained, as the CPU-time then is higher for the substructured model than for the original model.

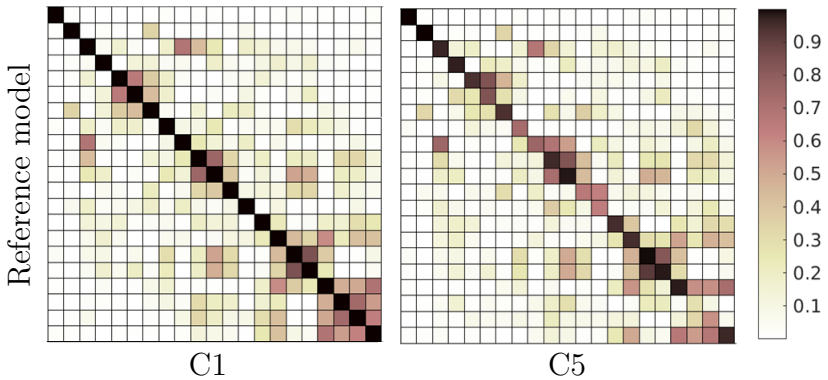

Figure 3.8: *MAC-correlation for the best (C1) and the worst (C5) configuration.*

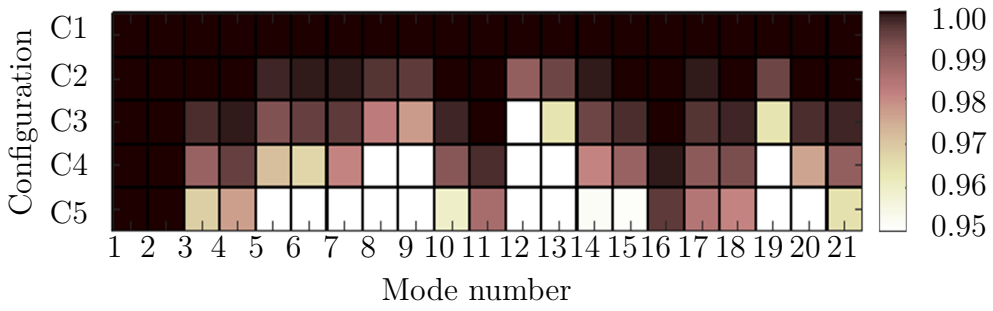

Figure 3.9: *Diagonal MAC-values for the different configurations.*

3.3.2 Reducing contact region

To reduce the number of interface DOFs, an analysis of the model is first performed where the reference model is excited with the reference load described in Section 3.2. The idea is to check if it is possible to reduce the contact region by first running a "pre-check" analysis, which can be done under linear conditions, to quickly identify the problematic areas for S&R issues. The critical areas are identified by analysing the gap between the two adjacent parts. A closed gap indicates that contact might occur. A MATLAB script is developed that detects all gap closures and reports the node numbers of the critical area. Once the areas are identified, new contact definitions are created.

The "pre-check" analysis shows that, for the reference load, contact only occurs in the zoomed in area of Figure 3.5. The contact definition is therefore redefined to this area only. For the frame the number of retained DOFs is now drastically decreased from 8 280 DOFs to 1 170.

3.3.3 Generation of substructures

The three main components are substructured with respect to the new contact definition discussed above. The substructures can be seen in Figure 3.10(a), 3.10(b) and 3.10(c). The red marks represent the retained nodes which are used to couple the substructures to each other through the rigid links. The black marks on the frame represent retained nodes to which the boundary conditions are applied, according to Section 3.1.2.2. The coloured lines represent the interfacing edges to the contact surfaces. Every node, with corresponding six degrees of freedom, along these lines are retained. The blue line corresponds to the interface of the frame and the orange line corresponds to the interface of the inner panel. Figure 3.10(d) shows the model to which the substructures are coupled. In addition to what is visible in the figure, 26 rigid links and 7 boundary nodes are also present. The model in Figure 3.10(d) is further referred to as the main model.

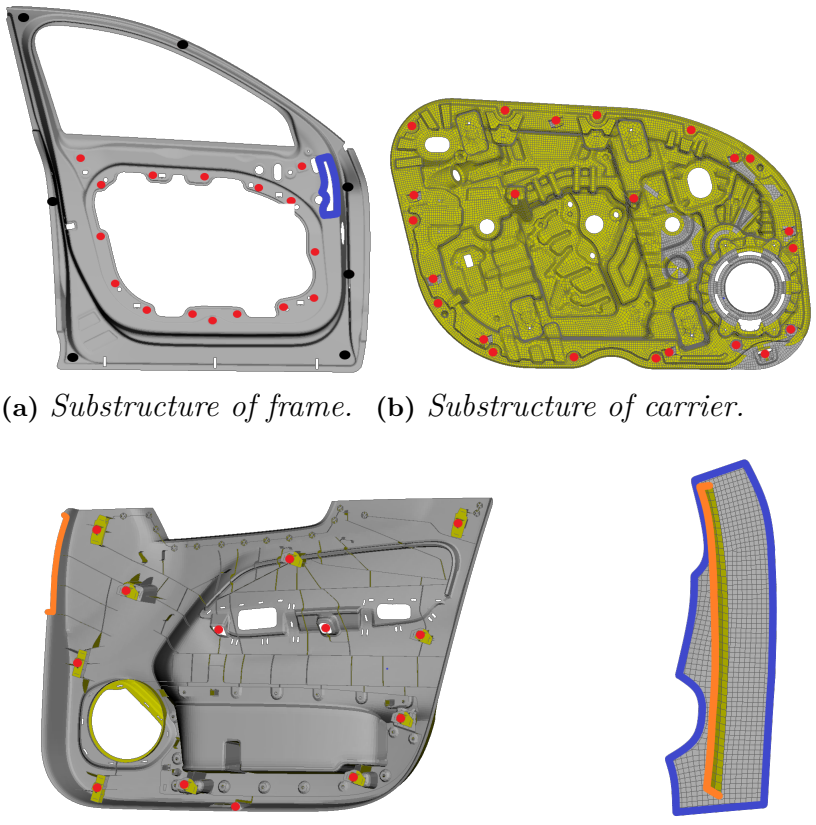

(a) *Substructure of frame.* **(b)** *Substructure of carrier.*

(c) *Substructure of inner panel.* **(d)** *Main model.*

Figure 3.10: *Main model and the three substructured components with respective retained DOFs highlighted.*

The first step of the substructure generation is to define the generalised DOFs representing the dynamic behaviour of the substructures. In this step, all retained DOFs are fully constrained, as described in theory Section 2.4.1.2. As discussed in Section 3.2, the maximum frequency of the excitation signal is 100 Hz. Using a multiple of 5 to account for nonlinearities gives the maximum frequency of interest as 500 Hz. When calculating the fixed interface vibration modes, the frequency range should be some factors higher than the frequency range of interest. Simone showed in his paper [31] that at least a factor of two should be considered. Since nonlinearities are present in the system, a factor of three is used which means that the generalised DOFs are calculated for frequencies up to 1500 Hz.

To make sure that the dynamic behaviour of the system is captured accurately for the specified frequency range, a study is performed where the frequencies in Table 3.6 are tested during the substructure generation. The table also shows the number of modes for each substructure in the specific frequency range.

Table 3.6: *Frequency study carried out for the fixed interface vibration modes. The table also shows the number of modes for the three substructures.*

Maximum frequency [Hz]	Frame[A]	Panel[B]	Carrier[C]
300	23	38	7
500	55	84	16
700	94	140	27
900	137	198	45
1 100	183	255	65
1 300	230	319	84
1 500	288	384	105
2 000	433	559	166

[A] Number of modes for the frame substructure.
[B] Number of modes for the panel substructure.
[C] Number of modes for the carrier substructure.

3.4 Distance from contact to substructures

As seen in Figure 3.10(d), only the elements for which contact is defined are left in the main model. Since the mass- and stiffness matrix for a substructure is updated only once, it will be constant during the nonlinear analysis. Only mass- and stiffness matrices for the elements kept in the main model are updated for every time step.

By varying the size of the panel substructure, it is possible to see whether the number of elements close to the contact region has a significant effect on the accuracy of S&R prediction. The initial substructured model, denoted at D8, can be seen in Figure 3.10. For this configuration, only the contact definition is kept in the main model, which represents a distance of 8 mm from the edge of the panel. The distance is then gradually increased by excluding elements from the inner panel substructure, leaving more elements in the main model. The procedure is schematically visualised in Figure 3.11. The different inner panel substructure configurations that are tested are presented in Table 3.7, where the number of interface DOFs and the total number of DOFs in the main model are presented.

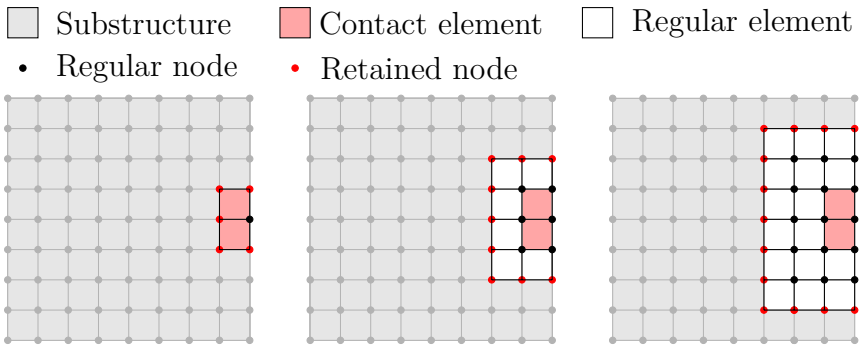

Figure 3.11: *Schematic visualisation of the study where the size of the panel substructure is varied.*

Table 3.7: *Different substructure configuration of the panel substructure.*

Notation	Distance from edge [mm]	# rDOFs[A]	Total # DOFs[B]
D8	8	372	7 866
D40	40	504	10 512
D90	90	696	16 170

[A] Number of retained DOFs for the panel substructure only.
[B] Number of DOFs in the assembled model.

3.5 Reducing the number of interface DOFs

Substructured systems that carries a high number of interface DOFs can be reduced further by using interface reduction techniques. A general way of doing this introduces generalised DOFs based on a calculated reduction basis [32]. However, this feature is not supported in ABAQUS. Therefore, the user has to output and reduce the global stiffness- and mass matrix. This, however, means that the modified matrices must be imported back to the solver which is only possible for mode based solvers [4]. Since the solver used for this thesis is not mode based, it is not possible to input the modified mass- and stiffness matrices back to ABAQUS. Therefore, the only way to reduce the number of retained DOFs, for the specific problem, is to use fewer coupling DOFs. However, randomly removing coupling DOFs as described in Section 3.3.1, gives an inaccurate modal behaviour.

This section describes two alternative approaches used to decrease the number of interface DOFs. These are both applied to the D8 configuration explained in Section 3.4, to see if the efficiency can be further improved.

3.5.1 Interface reduction based on modal behaviour

Instead of randomly removing retained interface DOFs, this part of the study aims to systematically decrease the number of retained DOFs based on the modal participation of each DOF at the contact interfaces. By solving the eigenvalue problem, according to theory Section 2.1, the eigenvectors for the requested frequency range are obtained. As the excitation signal has frequencies up to 100 Hz, the eigenvalue problem is solved for frequencies up to 100 Hz. Based on the normalised eigenvectors, the mean value for every DOF (mean value through all modes) is calculated. The absolute values of the eigenvectors are only considered. A low mean indicates that the DOF generally has a low contribution to the modes, in comparison to other DOFs. The idea is to remove the DOFs with lowest contribution. Further, some DOFs may have a high contribution for a single mode, and a lower contribution for the rest. Using only the mean value to remove the DOFs can therefore give an inaccurate modal behaviour. Therefore, the criteria for removing DOFs is also based on the maximum value for every DOF. The mean value for every DOF is calculated according to:

Table 3.8: *Configurations tested in the modal based interface reduction.*

Notation	η	# rDOFs frame[A]	# rDOFs panel[B]	Total reduction[C]
P25	25 %	1 102	322	7.65 %
P30	30 %	1 087	312	9.27 %
P35	35 %	1 038	304	12.97 %
P37	37 %	1 023	295	14.53 %
P40	40 %	1 011	285	15.95 %
P45	45 %	990	274	18.03 %

[A] Number of retained DOFs for the frame, corresponding Figure 3.10(a).
[B] Number of retained DOFs for the panel, corresponding Figure 3.10(a).
[C] Total reduction of number of retained DOFs.

$$\boldsymbol{x}^{mean} = \begin{bmatrix} \bar{x}_1 \\ \bar{x}_2 \\ \vdots \\ \bar{x}_m \end{bmatrix} = \frac{1}{n} \begin{bmatrix} |x_{1,1}| + |x_{1,2}| + ... + |x_{1,n}| \\ |x_{2,1}| + |x_{2,2}| + ... + |x_{2,n}| \\ \vdots \\ |x_{m,1}| + |x_{m,2}| + ... + |x_{m,n}| \end{bmatrix} \tag{3.1}$$

and the maximum value for every DOF is calculated as:

$$\boldsymbol{x}^{max} = \begin{bmatrix} \hat{x}_1 \\ \hat{x}_2 \\ \vdots \\ \hat{x}_m \end{bmatrix} = \begin{bmatrix} \max\{|x_{1,1}| \ |x_{1,2}| \ ... \ |x_{1,n}|\} \\ \max\{|x_{2,1}| \ |x_{2,2}| \ ... \ |x_{2,n}|\} \\ \vdots \\ \max\{|x_{m,1}| \ |x_{m,2}| \ ... \ |x_{m,n}|\} \end{bmatrix} \tag{3.2}$$

where in $x_{m,n}$, m represents the DOF number and n represents the mode number. The study is carried out for different factors (η) with respect to the 95^{th} percentile of the mean ($\boldsymbol{x}_{95}^{mean}$) and the maximum ($\boldsymbol{x}_{95}^{max}$). DOFs are removed if they satisfy the following conditions:

$$\begin{cases} x^{mean} \leq \eta x_{95}^{mean} \\ \quad \& \\ x^{max} \leq \eta x_{95}^{max} \end{cases} \tag{3.3}$$

The different values of η along with corresponding notation for the assembled system can be seen in Table 3.8.

3.5.2 Coarse mesh locally along the interface

Instead of leaving DOFs uncoupled, this part of the study aims to decrease the number of interface DOFs by instead coarsening the mesh. Since the mesh configurations at VCC follows certain guidelines and criterion, only the mesh along the contact interface is coarsened, in order to not modify the global mesh settings to a large extent. The mesh along the contact interface of only the frame is coarsened, since for the panel, contact is defined for two rows of elements only, which makes it difficult to coarsen the mesh without changing the contact elements significantly.

Table 3.9: *Mesh coarsening configurations of the frame with number of retained DOFs.*

Notation	# grouped elements	# rDOFs[A]	Total reduction[B]
M1	2	708	29.96 %
M2	3	558	39.69 %

[A] Number of retained DOFs for the frame only.
[B] Total reduction of retained DOFs, with all substructures included.

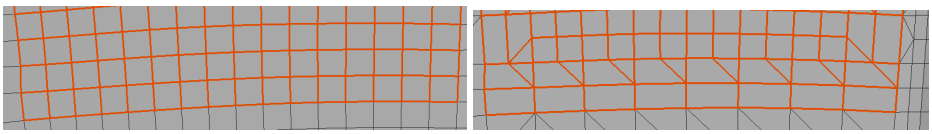

(a) Original mesh. **(b)** Coarsened mesh.

Figure 3.12: *Principle of local mesh coarsening. The left figure shows the original mesh for the contact elements. The right figure shows the mesh after it is locally coarsened.*

Two different mesh coarsening configurations are tested. The original size of the quadratic shell elements is 5 mm, and the new mesh configurations can be seen in Table 3.9., where M1 and M2 denotes the reduced models based on the coarsened mesh. When coarsening the mesh, the original elements along the contact interface are merged. The two different configurations represent 2 and 3 number of elements respectively merged into 1 element. Figure 3.12 visualises the principle in which the mesh is locally coarsened, where the elements highlighted in red are the elements for which contact is defined.

3.6 Contact definition on retained DOFs

In this section, the possibility of implementing another contact algorithm, by defining contact directly on the retained nodes, is discussed. This is done by using the NtS contact definition, which is described in theory Section 2.11. In order to model NtS contact, the slave surface is re-defined to a set of nodes along the edge of the panel as a node based surface. The new NtS contact definition can be seen in Appendix B, Figure B.1, where the nodes highlighted in red represent the nodes forming the contact surface. All these are defined as retained nodes in the substructure generation. The master surface is still defined as element based and it is highlighted in blue in Figure B.1. Even for this contact definition, the four different amplitudes presented in Table 3.4 are applied to see the influence of different levels of nonlinearity.

By using NtS contact definition, the entire panel is included in the substructure generation, which reduces the number of DOFs in the assembled system from 7 866 (for D8) to 7 332 which is a reduction of 6.79 %.

3.7 Verification

In order to evaluate the accuracy of S&R prediction for the reduced model, it is compared to the reference model. The results are compared using MATLAB. The verification procedure follows three main steps. The first two are based on the displacement response in a selected number of verification nodes. The nodes are located along the contact interfaces and are based on pairs in form of "master and slave" nodes. The verification nodes can be seen in Appendix C, Figure C.1 where the yellow marked nodes corresponds to the master nodes (located on the frame) and the blue marked nodes corresponds to the slave nodes (located on the inner panel). The set consists of 88 nodes, i.e. 44 node pairs.

3.7.1 Modal behaviour comparison

The first step of the verification procedure is to compare the modal behaviour of the substructured system with the modal behaviour of the reference model. This is done by means of eigenvector comparison. Solving the eigenvalue problem disregards all kinds of nonlinearities. For this step, modes up to 100 Hz are compared. As described in Section 2.6.1, the eigenvectors are compared using MAC. The eigenvectors are based on 264 DOFs, since three translational DOFs are requested for the 88 nodes.

3.7.2 Comparing frequency response

As for the nonlinear analyses, the reduced model is compared based on the frequency response. The system is excited with frequencies in the range 0-100 Hz, and the sampling frequency is, as discussed in Section 3.2, set to 1000 Hz. Based on the Nyqvist theorem, frequency content up to 500 Hz is obtained when transforming from time domain to frequency domain. As described in Section 2.3, the transfer function is obtained in the frequency domain by dividing the output with the input. This requires for both the input and output to have the same frequency range. Hence, it is not possible to calculate the transfer functions for the entire frequency range, but only up to 100 Hz. Since the purpose of this verification step is to compare the models with respect to nonlinear effects, the frequency output up to 500 Hz is instead compared.

The verification node set consists of the 88 nodes. During this verification step though, the relative displacement between the master- and slave node is analysed which in total gives 44 frequency responses. The responses are compared using the normalised root mean square error, described in Section 2.6.2, which based on two vectors as input gives a scalar value between minus infinity and one. Comparing the frequency responses of the relative displacement for all 44 node-pairs separately, for X-, Y- and Z-direction, would result in 132 scalar values of NRMSE. Instead, the data is rearranged into one vector containing values for all node-pairs in all directions. This allows for two models to be compared by mean of normalised root mean square error, with only one scalar value as output.

3.7.3 Contact force

The last step of the verification procedure is to check how accurately the reduced models predict contact. This is done by calculating the contact normal force along the elements where contact is defined for the inner panel, which gives 44 contact forces as function of time. For this step, the following three parameters are analysed and compared:

- Time of contact events
- Number of contact events
- Amplitude of contact forces

Since the highest contact force generates the loudest S&R, the maximum force in each time step is compared. i.e, when comparing the reduced model with the reference model, two data points are not necessarily based on the force in the exact same node.

When comparing contact force with respect to time, a difference less than 10 ms between the models is considered precise. When comparing the two models by means of contact force amplitude, the mean value of all common contact events is calculated and compared. For comparison of single contact events, the amplitude prediction is considered precise if the absolute difference between the reduced model and the reference model is less than 5%.

4
Results & discussion

This section presents the results from the different studies explained in the method chapter. First, the results are presented from the study where different frequency ranges are tried out for fixed interface vibration modes. Next, the results from changing the size of the inner panel substructure are presented. After that, the results from the redefined interface configurations are described. Finally, the alternative contact algorithm of NtS is discussed.

4.1 Fixed interface vibration mode range

To get an idea of how the frequency range of the fixed interface vibration modes affects the dynamic behaviour of the reduced model, different frequency ranges are tried out as described in Section 3.3.3. Figure 4.1 shows NRMSE values for all configurations, each based on the four different excitation signals A1-A4. For A1, the NRMSE values improve significantly between 300 Hz and 900 Hz. Between 900 Hz and 1 100 Hz a small difference can be seen. After that there is no significant improvement with an increasing frequency. As there is no contact for A1, skipping the nonlinear multiple of 5 would result in a maximum frequency of 200-500 Hz using general recommendations. Figure 4.1 shows that this is not enough to maximise the accuracy of the model.

For A4, changes in NRMSE value can be seen until a frequency of 1 300 Hz, since increasing the frequency from 900 Hz to 1 100 Hz decreases the accuracy slightly. Hence, the maximum frequency of the excitation signal needs to be multiplied by at least a factor of 13 for A4 to maximise the accuracy. For A1-A3 however, a factor of 11 is enough. The CPU-time for the different frequency configurations can be seen in Table 4.1. By lowering the frequency from 1 500 Hz to 1 300 Hz for the fixed interface vibration modes, the CPU-time can be reduced by 3.5 %.

Table 4.1: *CPU-time for different frequency ranges of the fixed interface vibration modes.*

Frequency [Hz]	300	500	700	900	1 100	1 300	1 500	2 000
CPU-time [10^3 s]	8.44	8.71	8.89	9.07	9.20	9.52	9.87	10.79

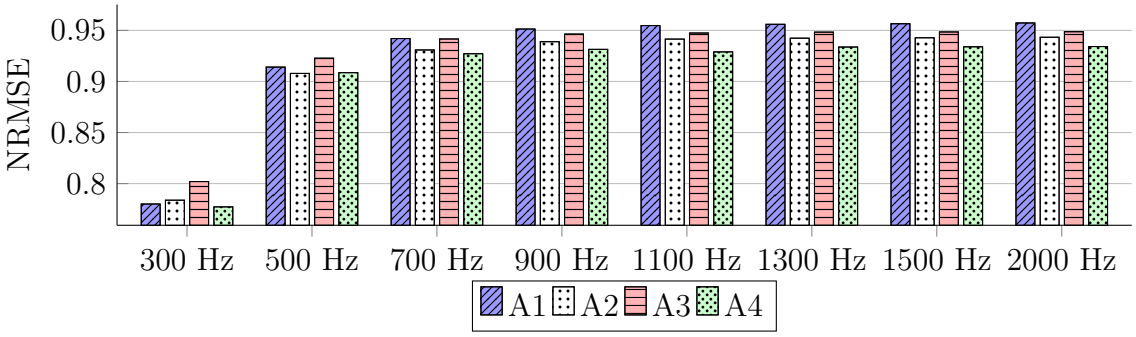

Figure 4.1: *NRMSE for different frequency ranges for the fixed interface vibration modes.*

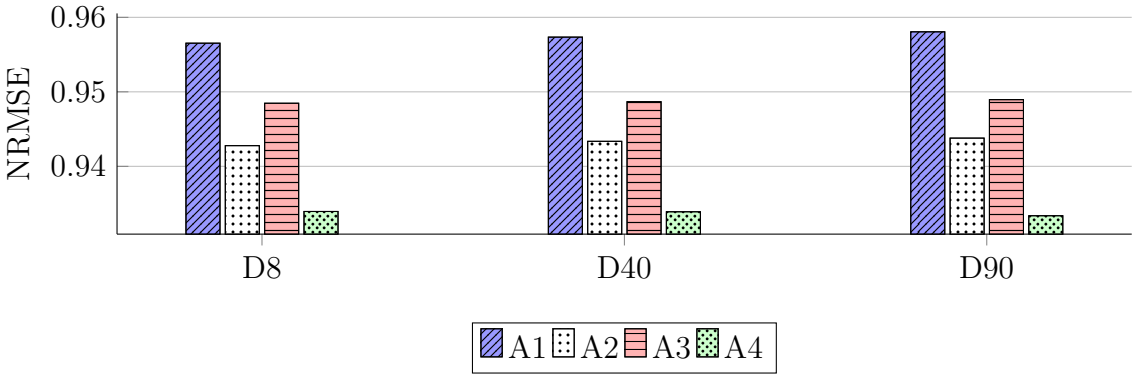

Figure 4.2: *NRMSE for the different distance configurations.*

4.2 Distance from contact to substructure

As described in Section 3.4, the distance from the panel-substructure to the contact interface is varied in order to see if the number of elements close to the contact interface has any effect on the accuracy. The different configurations can be seen in Table 3.7. Figure 4.2 shows the NRMSE for the three configurations where it can be seen that there is almost no difference between D8, D40 and D90. Some minor improvements can be seen for A1-A3 when increasing the distance from the contact interface. For amplitude level A4 the NRMSE is the same for D8 and D40 while it decreases slightly for D90. It is noted that for all three configurations, A1 has the best NRMSE and A4 has the worst. The NRMSE for A3 is for all configurations better than the NRMSE for A2.

Table 4.2: *NRMSE for D8 in X-, Y- and Z-direction separately for different amplitudes.*

Amplitude	X	Y	Z
A1	0.9479	0.9600	0.9497
A2	0.9208	0.9505	0.9360
A3	0.9193	0.9586	0.9457
A4	0.8813	0.9521	0.9419

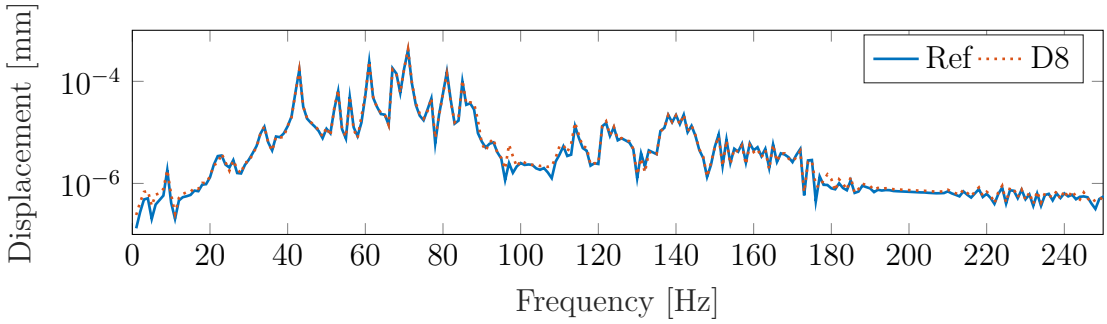

Figure 4.3: *Frequency response of relative displacement in X-direction for excitation signal A1.*

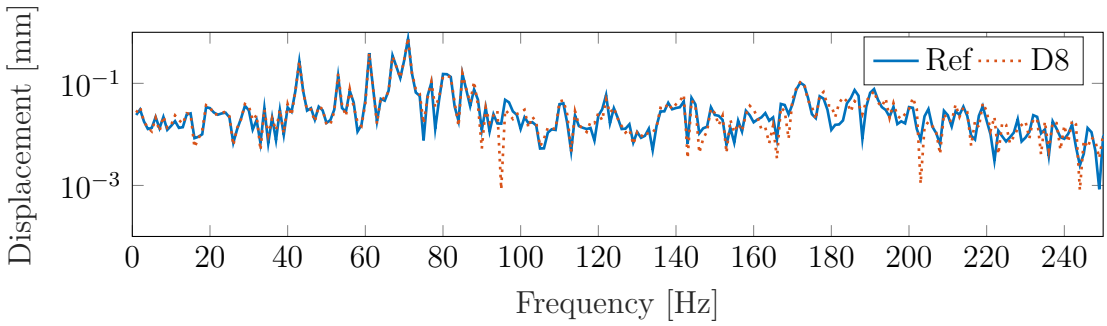

Figure 4.4: *Frequency response of relative displacement in X-direction for excitation signal A4*

The frequency responses of the relative displacement in X-, Y- and Z-direction for D8 are compared separately to see the influence of the amplitude in the different directions. The results can be seen in Table 4.2. For all amplitudes, X-direction lowers the total NRMSE, and it decreases significantly when the scaling of the excitation signal is increased. This is not the case for Y- and Z-direction, where the scaling of the excitation signal does not have a significant affect on the accuracy. The frequency response in X-direction for D8 with amplitude A1 for frequencies up to 250 Hz, can be seen in Figure 4.3 and the frequency response for A4 can be seen in Figure 4.4. For A1, the behaviour of the reference model and the reduced model is similar with some small differences in the frequency range of 90-110 Hz. For A4 though, there is visible differences in amplitude already at 40 Hz. For frequencies above 90 Hz, the two models behave differently, lowering the NRMSE value.

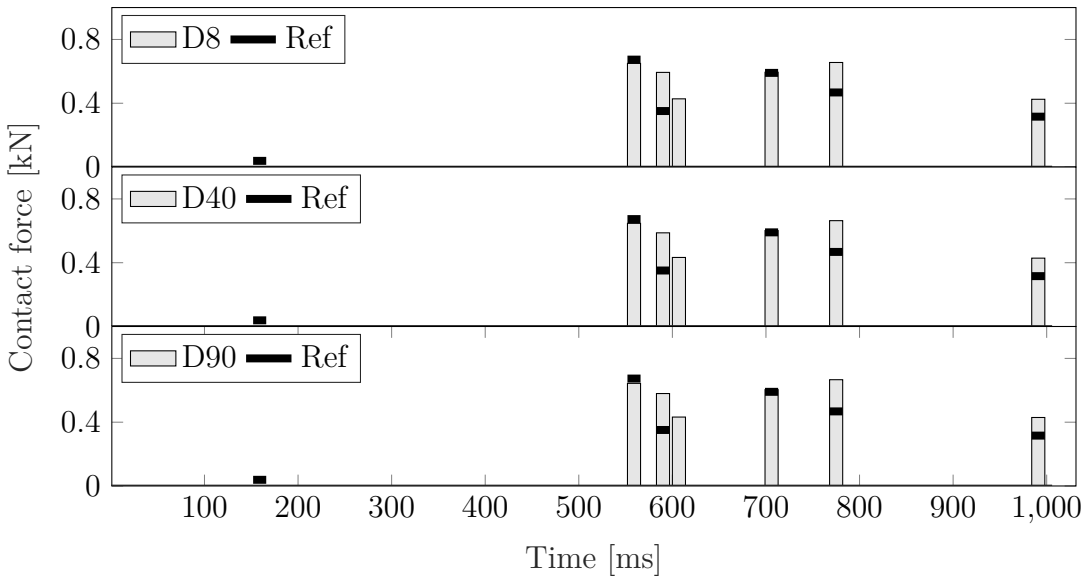

Figure 4.5: *Contact events when the system is excited with amplitude A2. Contact force for D8, D40 and D90 represented by the grey bars. Contact force for the reference model represented by the black markers.*

The maximum contact force as function of time for D8, D40 and D90 can be seen in Figure 4.5, when the system is excited with amplitude A2. The black markers represent contact events for the reference model and the grey bars represent contact events for the reduced model. The top plot shows the time and amplitude of the contact events for configuration D8. The middle plot shows corresponding for D40 and the bottom one for D90. As can be seen when comparing the three plots, there is no significant difference. All three reduced models misses the first contact event. They all capture two contact events perfectly both with respect to time and amplitude. The rest of the events are captured perfectly with respect to time but not with respect to amplitude, as they all predict higher contact force amplitudes. D8 predicts the mean amplitude 21.7 % higher than the reference model. D40 predicts the mean amplitude 22.1 % higher and D90 predicts it 21.9 % higher. The maximum difference between the reduced models and the reference model can be seen at 590 ms, where D8 predicts the amplitude 69.0 % higher. D40 predicts the same event 67.3 % higher and D90 predicts it 65.1 % higher.

The contact force when the systems are excited with amplitude A3 can be seen in Figure 4.6. They all predict contact at the time points 80 ms and 905 ms, which the reference model does not. As for the rest of the predictions, all three reduced models capture all contact events with respect to time, but generally with a higher contact force amplitude than the reference model. D8 generally predicts 18.2 % higher amplitude, D40 generally predicts 19.3 % higher and D90 predicts 21.9% higher. At time 490 ms, D8 predicts an amplitude 33.5 % lower than the reference model, meanwhile D40 and D90 predicts it perfectly with differences of only 3.97 % & 3.3 % respectively. At time 590 ms however, D90 predicts the amplitude 51.5 % higher than the reference model, meanwhile D8 and D40 predicts it 13.8 % & 12.9 % higher.

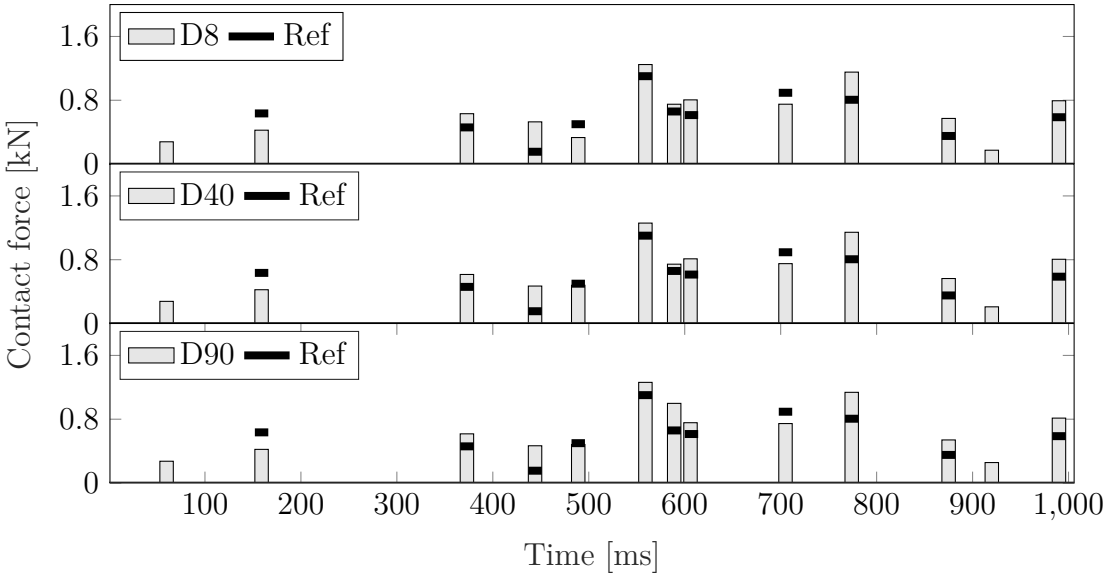

Figure 4.6: *Contact events when the system is excited with amplitude A3. Contact force for D8, D40 and D90 represented by the grey bars. Contact force for the reference model represented by the black markers.*

The contact force for A4 is shown in Figure 4.7, where it can be seen that all three reduced models predict the same number of contact events, at the same time points as the reference model. Here, the contact force amplitude prediction of the reduced models is better than for A2 and A3. D40 predicts the mean amplitude only 2.5 % higher than the reference model. D8 predicts the mean amplitude 6% higher and D90 predicts it 6.5 % higher. Comparing the contact event at time 773 ms for D90 with corresponding for D40 and D8, one can see that D90 captures the amplitude of the contact perfectly meanwhile D8 and D40 predict the amplitudes 50.8 % and 64.4 % lower. For the contact force at time 560 ms all reduced models predict a low amplitude in comparison to the reference model. However, the prediction for D90 is 41.6 % lower meanwhile it is 25.41 % lower for D8 and 25.4 % lower for D40. For the rest of the contact events, the reduced models behave similarly.

The accuracy of S&R prediction for A4 is better than for A2 and A3, despite the low NRMSE values. Table 4.2, shows that the lowest NRMSE is calculated for X-direction, which in turn lowers the total NRMSE. The highest NRMSE value is identified in Y-direction. Since the two adjacent parts have an initial gap of 3.7 mm in Y-direction, the majority of the contact impacts are based on the relative Y-directional movement. This can be an explanation to why the A4 configuration is able to predict contact as good as for A2 and A3. Comparing the frequency response for D8 in X-direction with the reference, shown in Figure 4.3 and 4.4, shows that the largest difference in response can be seen for frequencies above 90 Hz. Since the maximum frequency of the excitation signal is 100 Hz, it is likely that the frequencies to generate most of the contact events are located below 100 Hz. This can also be an explanation to why the reduced model is able to predict contact for A4, despite the low NRMSE which is based on a comparison for frequencies up to 500 Hz.

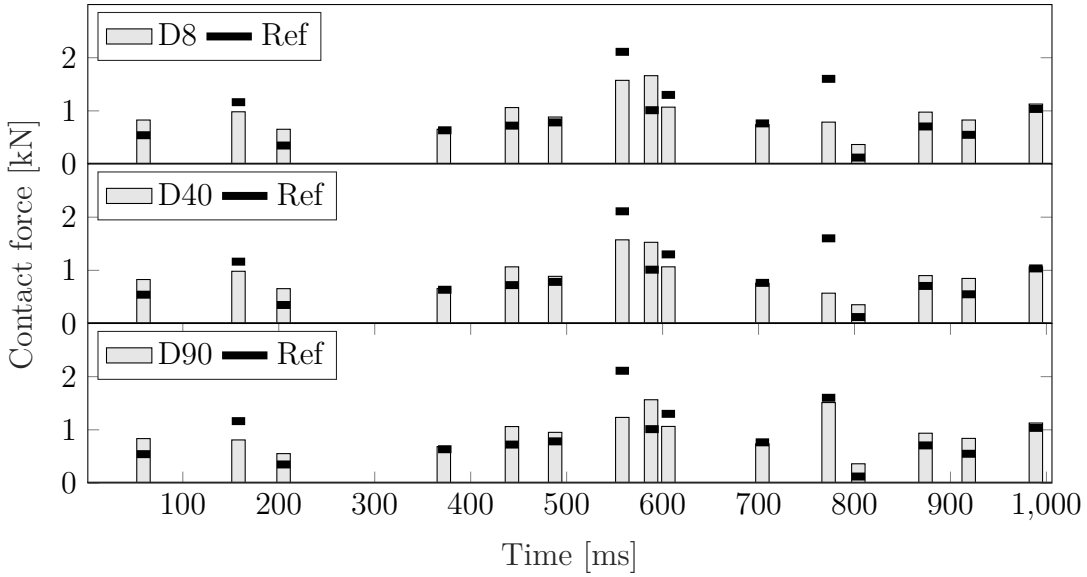

Figure 4.7: *Contact events when the system is excited with amplitude A4. Contact force for D8, D40 and D90 represented by the grey bars. Contact force for the reference model represented by the black markers.*

Table 4.3: *Comparison of amplitude for the contact force between D8 and the reference model.*

Status of amplitude prediction	A2	A3	A4
# perfect predictions[A]	2	1	4
# predictions too low	0	3	4
# predictions too high	3	7	7

[A] Differences of less than 5 % compared to the reference model.

For some occasions, the reduced models predict contact when the reference model does not. For A2, they predict one extra event and for A3 they predict 2 extra. However, for A4 the reduced models and the reference model predict the same number of events at the exact time points. Hence, the accuracy does not seem to decrease with an increasing amplitude of the excitation signal but rather the opposite. Comparing the amplitudes of the contact forces, the D8 generally has higher amplitude compared to the reference model according to Table 4.3. However, for some occasions it predicts lower amplitudes as well. The differences are generally small, but one explanation to this phenomena can be a shift in time between the reduced model and the reference model. As discussed in Section 1.3, a limitation of the thesis is the time steps and the output frequency. The maximum output frequency is 1000 Hz. However, based on 1000 Hz the output contact forces consist of peaks based on few data points. Hence, the calculated maximum amplitudes are not completely reliable, but can rather be used as an indicator for contact prediction.

Table 4.4: *CPU-time for the different configurations.*

Configuration	CPU-time [10^3 s]
Ref	463.45
D90	13.54
D40	10.96
D8	9.87

The influence of increasing the distance from the interface between the substructure and the contact region does not have any significant affect on the accuracy of contact prediction. Approximately D8, D40 and D90 all have the same accuracy in predicting contact with respect to time, independent of excitation signal. For one or two peaks, D90 has a better prediction than D8 considering amplitude. This might have to do with the fact that for the D90 configuration, a larger portion of the original model is kept, which better represents the original system. Table 4.4 shows the computational time for the reference model and the three substructured models. All three configurations have a CPU-time significantly lower than the reference model. As expected, D8 has the lowest CPU-time. The CPU-time for D8 is 27.1 % lower than for D90.

4.3 Reducing the number of interface DOFs

This section presents the results from the reduction of DOFs along the contact interfaces. The results from the reduced interface configurations are compared to D8, which has an unmodified mesh size and where all substructures are fully coupled. Based on the initial contact definition, seen in Figure 3.7(a), the reduced model surprisingly has a significantly higher computational cost than the reference model. For problems including large contact definitions it is therefore important to either reduce the size of the contact regions, or to reduced the number of retained DOFs.

4.3.1 Interface reduction based on modal participation

As described in Section 3.5.1, interface DOFs are removed based on the 95^{th} percentile value of the maximum and mean of the eigenvectors. The different configurations can be seen in table 3.8. Table 4.5 shows the lowest diagonal MAC-value for all configuration with respective mode number. For P45, the lowest MAC value is identified for the 9^{th} mode as 0.9284, which is significantly lower compared to the other configurations. P25, P30, and P35 are similar as the lowest MAC-values are close to 1, and are identified for mode 21. For P37, P40 and P45 the lowest MAC-values are identified for mode 8-9.

Table 4.5: *Lowest diagonal MAC value and corresponding mode number.*

	P25	P30	P35	P37	P40	P45
Lowest diagonal MAC-value	1	1	0.9994	0.9966	0.9916	0.9284
Corresponding mode number	21	21	21	8	8	9

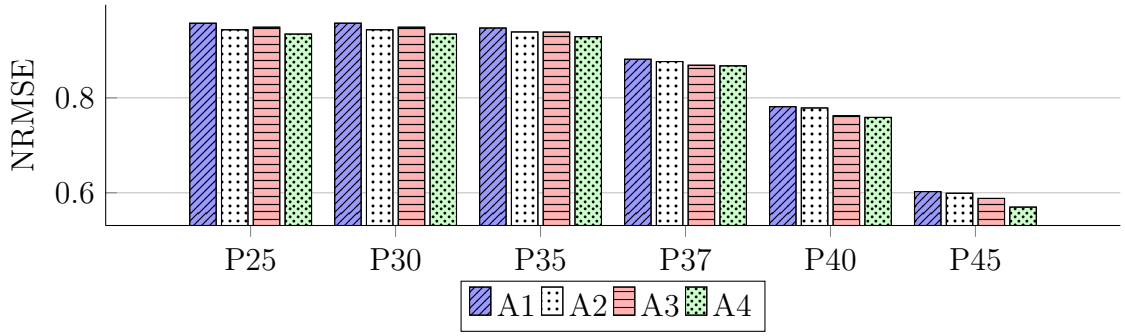

Figure 4.8: *NRMSE for P25-P45 based on excitation signals A1-A4.*

The NRMSE values for the different configurations can be seen in Figure 4.8 where one can see that the values, as expected, decreases with a lower number of interface DOFs. Similar to the results for D8, see Section 4.2, A1 has the best NRMSE and A4 has the worst for for all configurations. For A2 and A3 though, the reduction of retained DOFs affects the NRMSE in the sense that after P35, the NRMSE is better for A2 than for A3, which was not the case for D8. No significant difference can be seen between P25, P30 and P35. However, for P37, P40 and P45 a gradual reduction is noticed.

Figure 4.9 shows the contact force as function of time for P35 and amplitudes A2-A4. Comparing this with the results for D8, in Figure 4.5, 4.6 and 4.7, one can see that they capture the same amounts of contact events for all amplitudes. This is despite the fact that P35 carries 200 coupling DOFs less than D8. For some contact events such as the event occurring at 560 ms for amplitude A3, D8 captures the amplitude slightly better than P35. P35 predicts the amplitude 33.8 % lower meanwhile D8 predicts it 13.3 % higher than the reference model. The result shows similar accuracy for A2-A4.

For P37 the correlation considering contact prediction is inaccurate, as can be seen in Figure 4.10. The reduced model only captures 1 out of the 6 contact events for A2, and the predicted amplitude is significantly lower than for the reference. Even for A3 and A4 the model is inaccurate as it misses a lot of the contact events. The configuration only has 24 coupling DOFs less than P35, which shows how sensitive the substructured model is with respect to skipping coupling DOFs. The drawback of this method is that it is highly dependent on the model and its modal behaviour. It can also be sensitive to higher frequencies as smaller wave-length tend to give higher contribution for the rotational DOFs.

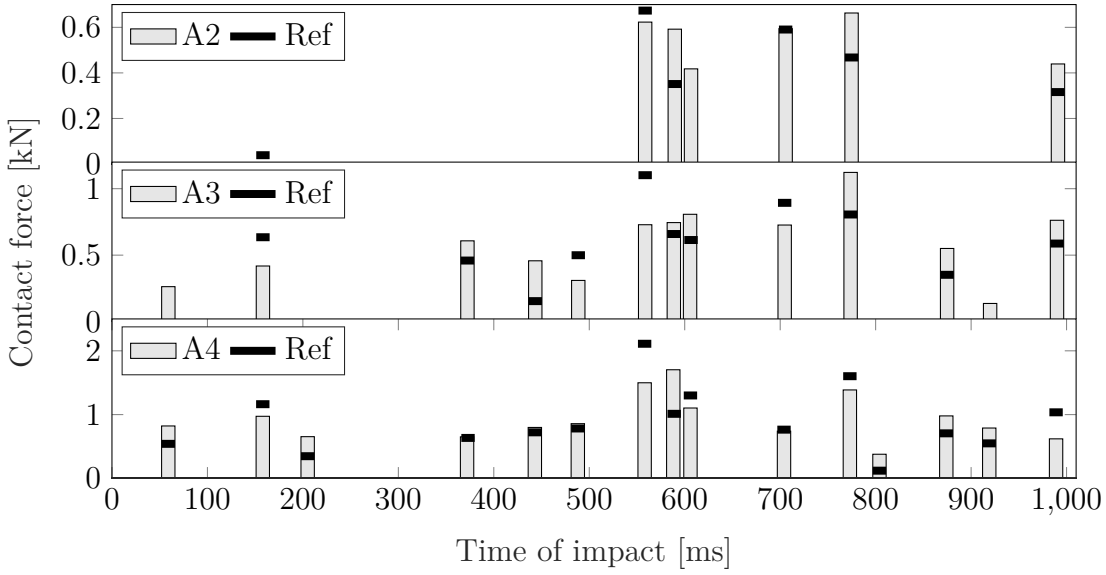

Figure 4.9: *Contact force as function of time for interface reduction configuration P35.*

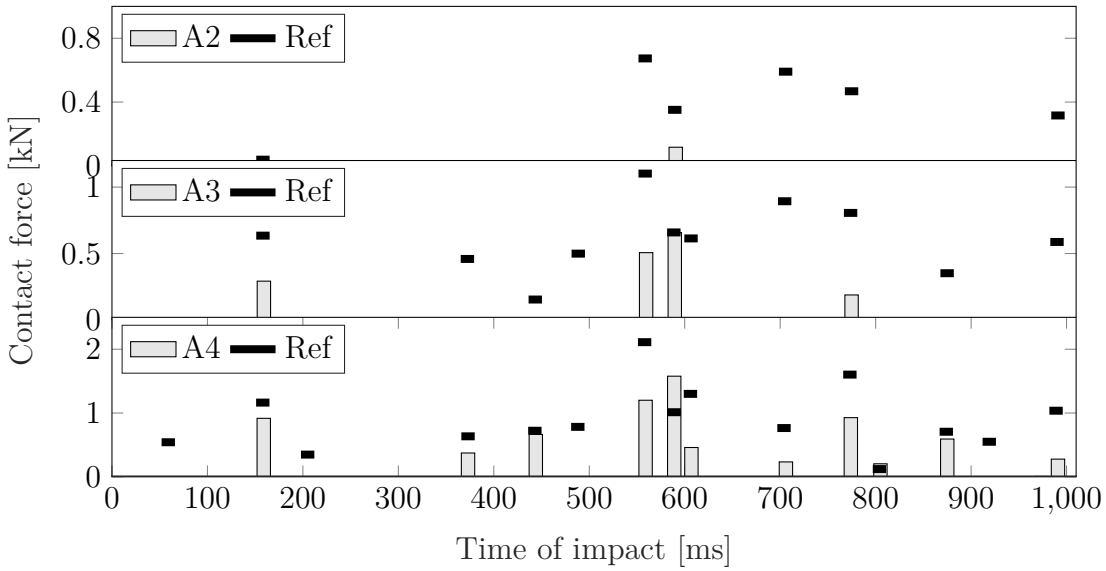

Figure 4.10: *Contact force as function of time for interface reduction configuration P37.*

4.3.2 Coarse mesh locally along the interface

This section presents the results from the interface reduction based on local mesh coarsening along the interface of the frame substructure. For M2, the number of interface DOFs for the frame is reduced by 52.3 %. The reduction of the total number of retained DOFs is 39.7 %, without leaving any DOFs uncoupled. This section presents the accuracy of corresponding model.

The NRMSE values for D8, which corresponds to the reduced model of the original mesh size, are presented in Figure 4.11, along with the NRMSE values for M1 and

M2. Comparing the models, it can be seen that M1 and M2 are similar to D8, with a minor reduction in NRMSE. The influence of the amplitude does not have any significant affect since similar change can be seen for A1-A4.

The contact force as function of time for M2 can be seen in Figure 4.12, for A2-A4. Comparing this with the results for D8, shown in Figure 4.5, 4.6 and 4.7, one can see that they are similar as they capture the same amount of contact event with approximately same precision in amplitude. For A3 at time 590 ms though, M2 predicts the amplitude 52.7 % too high, meanwhile D8 only predicts it 13.8 % too high. As for A4 a small difference can be seen at time 570 ms. This time M2 predicts the amplitude 52.2 % too low and D8 predicts it 25.5 % too low.

A drawback of local mesh coarsening is that it generates a significant amount of triangular elements around the interface. VCC has certain guidelines for how to construct the mesh in order to easily share models between departments. Therefore, locally changing the mesh can generate problems if the model or the substructures are to be shared. Also, as described in theory chapter 2.11, the NtS contact definition is highly dependent on the mesh. Hence, coarsening the mesh can generate

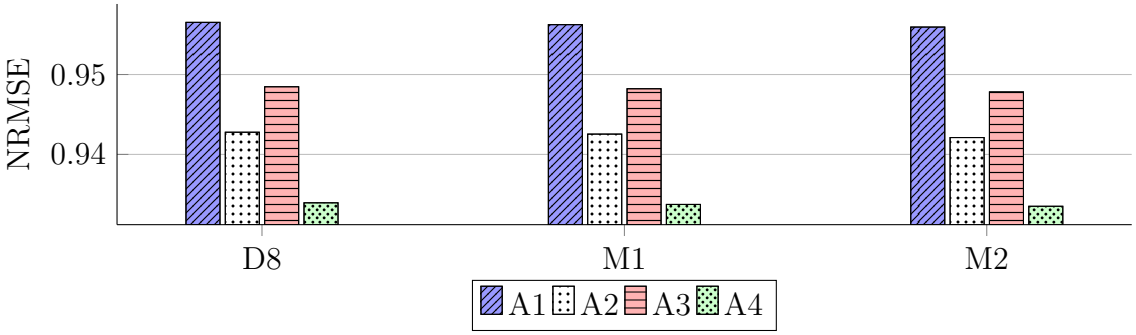

Figure 4.11: *NRMSE value comparison of normal and coarse meshed model.*

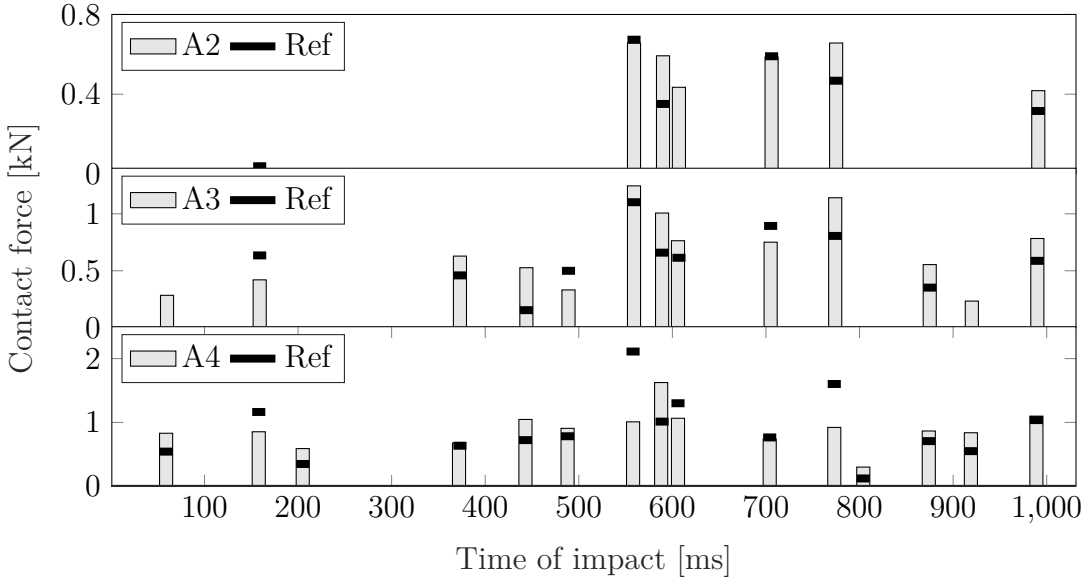

Figure 4.12: *Contact force as function of time for coarse mesh configuration M2.*

inaccurate contact predictions for this type of contact definition. For the panel, contact is defined only for two rows of elements. It is therefore not possible to apply the local mesh coarsening without generating triangular elements in a large portion of the contact elements.

4.4 Contact definition on retained DOFs

This section describes the results corresponding to the NtS contact definition discussed in section 3.6. Figure 4.13 shows the difference in contact prediction between the StS contact definition and the NtS definition. The NtS definition generally predicts the amplitude 68.4 % higher for A2, 73.1 % higher for A3 and 42.3 % higher for A4. NtS also predicts one extra contact event for load A2 at time 610 ms. For load A3, NtS misses the contact at time 875 ms and predicts an extra contact event at time 920 ms. For load A4, the NtS predicts two extra contact events at time 175 ms and 920 ms. Generally the two different methods are similar at predicting contact with respect to time, but not with amplitude. Which one of these that best represents reality is out of scope for this thesis.

Figure 4.14 shows the NRMSE values for the models based on NtS contact definition and the models based on StS contact definition. As can be seen, there is no significant difference between NtS and StS for amplitude A1. For A2 and A3, a minor difference can be seen. For A4 though, a large difference can be seen as NtS has a 27 % lower NRMSE.

A closer analysis of NtS for A4 shows that the NRMSE values in all directions (X, Y and Z) are low. Table 4.6 shows the NRMSE values for respective direction, which shows that, once again the relative displacement in X-direction has the worst correlation. Z-direction has the best correlation, but it is still bad in comparison to StS.

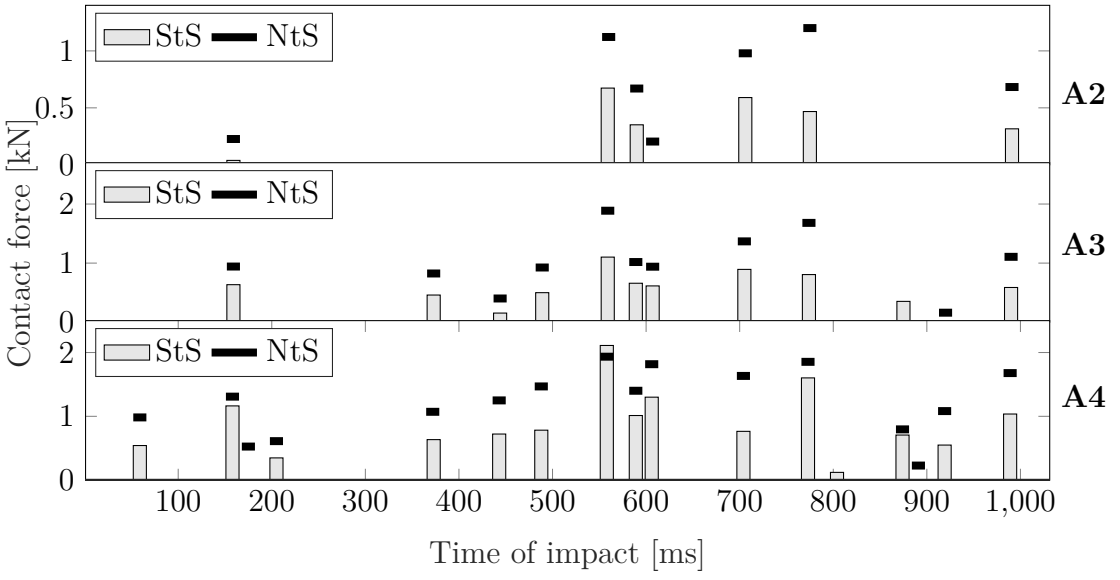

Figure 4.13: *Contact force as function of time for NtS and StS.*

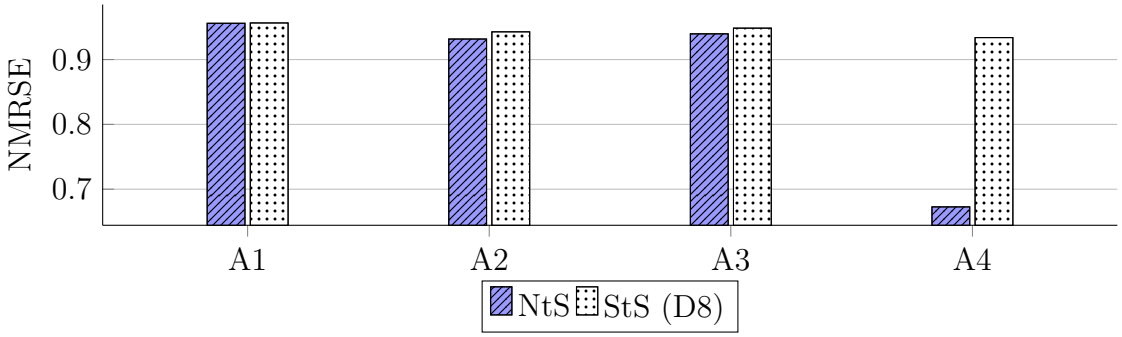

Figure 4.14: *NRMSE comparison between StS and NtS.*

Table 4.6: *NMRSE for A4 in X-, Y- and Z-direction separately.*

	X	Y	Z
NRMSE	0.5751	0.6770	0.8318

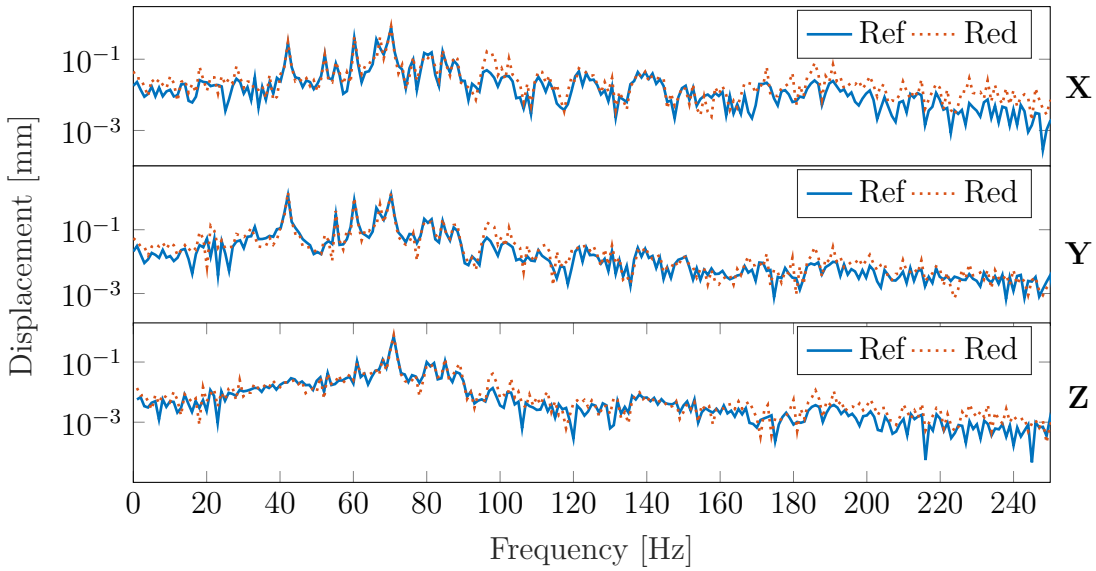

Figure 4.15: *Frequency response of NtS contact definition for A4.*

Analysing the frequency responses in respective direction, which can be seen in Figure 4.15, it can be seen that for frequencies up to 40 Hz, all directions have a bad correlation with the reference model although they all capture the highest peaks accurately. For frequencies above 160 Hz, again they all have a bad correlation. Compared to the frequency response functions in X-direction for the StS configuration (D8), the NtS frequency response shows a low correlation for a wider frequency range.

Figure 4.16 shows the contact force as function of time for the reduced NtS based model and corresponding reference model. The reduced model is, for A2-A4, accurate with respect to contact prediction in time, but not in amplitude as it predict the amplitude significantly higher. The reduced model generally predicts the amplitude

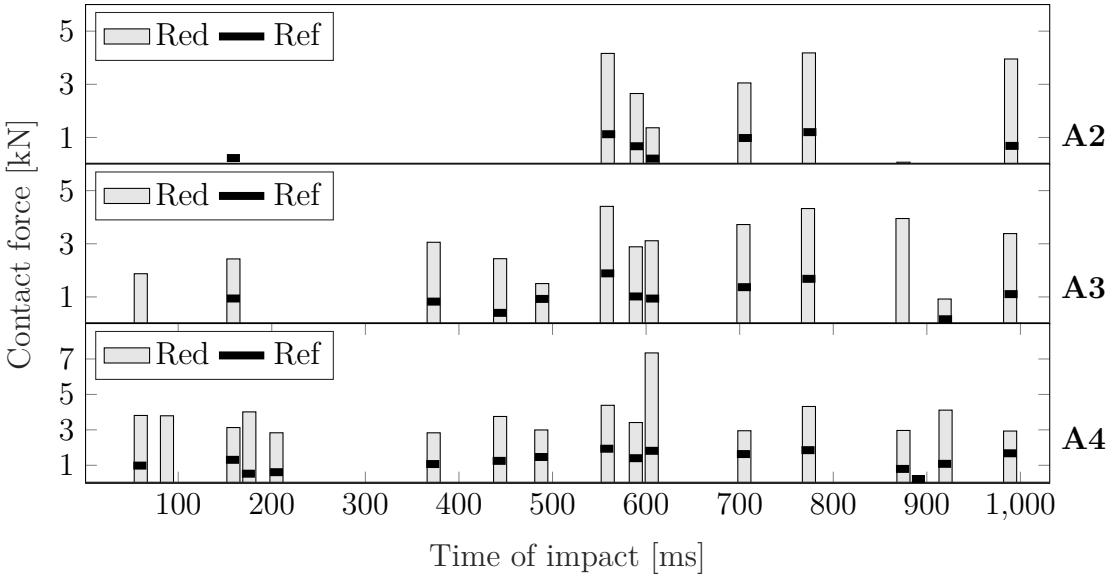

Figure 4.16: *Contact force as function of time for NtS reference and reduced model.*

338.4 % too high for A2, 181.9 % too high for A3 and 174.2 % too high for A4. For amplitude A3, the reduced model identifies two extra contact events at time 60 ms and 874 ms. For load A4, the reduced model identifies one extra contact event at time 88 ms and misses one contact event at time 890 ms.

4.5 Computational time

Based on the results in above sections, the most efficient configurations, with respect to time and accuracy, are calculated on the same machine using the same number of CPUs to compare the CPU-times. The results can be seen in Table 4.7.

Keeping only the contact elements in the main model with all DOFs coupled, corresponding to configuration D8, decreases the computational time with 97.9 %. Still, D8 is able to predict all contact events with respect to time, with an exception for a single contact event when the system is excited with amplitude A2. The contact force amplitudes predictions though is generally too high.

For the specific case, decreasing the number of retained DOFs by leaving some DOFs uncoupled based on the modal behaviour, lowers the CPU-time with 3.2 % (compared to D8). Leaving more DOFs uncoupled gives inaccurate results. The mesh coarsening however, decreases the CPU-time significantly according to Table 4.7, without sacrificing the accuracy of contact prediction. By coarsening the mesh, the number of retained DOFs is successfully decreased by 39.7 %, without leaving any DOFs uncoupled. This saves additional 32.5% in CPU-time (compared to D8). However, one have to keep in mind that the mesh coarsening also lowers the total number of DOFs in the model by 15.3 %. Hence, the lowering of CPU-time for M2 is not only affected by the number of retained DOFs but also of the total number of DOFs in the model.

The study of the fixed interface vibration mode range shows that there is no significant improvement in NRMSE between 1 300 Hz and 1 500 Hz. Hence, by lowering the frequency range from 1 500 Hz to 1 300 Hz, the CPU-time can be lowered by 3.5 %, which is higher than the the modal based interface reduction.

Comparing the CPU-time for the NtS based reduced model, with the StS based, there is no large difference. The NtS based has a CPU-time only 2.7 % less than the StS based, and the accuracy is significantly worse considering contact force amplitude.

Table 4.7: *Summary of size and CPU-time for the different configurations.*

	Ref_{StS}[B]	D8_{StS}	P35_{StS}	M2_{StS}	Ref_{NtS}[C]	Red_{NtS}
# rDOFs (panel)	-	372	304	372	-	342
# rDOFs (frame)	-	1 170	1 038	558	-	1 170
Total # DOFs[A]	1 169 406	7 866	7 866	6 666	1 169 406	7 332
CPU-time [$\cdot 10^3$ s]	463.45	9.87	9.55	6.66	453.51	9.61

[A] Total number of DOFs in the assembled model.
[B] StS denotes the models with surface-to-surface based contact definitions.
[C] NtS denotes the models with node-to-surface based contact definitions.

5
Concluding remarks

5.1 Conclusion

The purpose of this thesis was to increase the understanding for if, and how, the CMS-method of Craig-Bampton can be used for S&R simulations including local nonlinearities in the form of contact. The results clearly showed that the substructured model was accurate in prediction of contact with respect to time. As for the prediction of contact force amplitude, the substructured model generally predicted higher amplitudes, even though the differences were not large between the reference- and the substructured model. However, for a sampling frequency of 1000 Hz the contact force amplitudes consisted of few data points. This made the amplitude predictions not completely reliable, but rather useful as an indicator for contact. The total CPU-time for the reduced model was lowered by 97.9 % compared to the reference model.

Further, the results showed that the substructured model was more accurate at predicting contact for "surface-to-surface" based contact definitions than for "node-to-surface" based, as the latter predicted significantly higher amplitudes.

Finally, it was found that the number of retained DOFs for the substructure showed to have large impact on the computational cost in ABAQUS. Substructuring models with large contact regions might therefore have an opposite effect as it instead can increase the computational cost. However, redefining the contact region by first identifying critical areas for S&R showed to decrease the CPU-time drastically. Further, the number of interface DOFs could be decreased by either coarsening the mesh locally around the contact interfaces, or by leaving DOFs uncoupled from the rest of the model based on their mode-shape contribution. The latter had a small effect on the computational time, since only a small portion of DOFs could be left uncoupled without sacrificing the accuracy of contact prediction. The interface between the substructures and the contact region showed to be sensitive to uncoupled DOFs. However, locally coarsening the mesh showed to save additional 32.5 % in CPU-time, without sacrificing contact prediction.

5.2 General recommendations

It was observed during this thesis that the Craig-Bampton method works well for systems including nonlinearities in the form of contact, if the contact is based on

StS definition. It is not recommended to define the contact directly on the retained DOFs, using the NtS based contact definitions. If using the StS definition, the number of elements close to the contact region does not have any significant effect on the accuracy of S&R prediction. Hence, it is recommended to couple the substructures directly to the elements for which contact is defined, in order to minimise the number of DOFs in the assembled model. Since it was observed that the CPU-time was dominated by the number of interface DOFs it is further recommended to use mesh coarsening to reduce the number of interface DOFs.

5.3 Future work

This section gives some proposals on future studies within the area of using substructures in S&R simulations including nonlinearities in the form of contact. The proposals are based on ideas that have been discussed during the thesis, but that due to limitations, have not been carried out.

During this thesis, the time steps of the analyses was based on a sampling frequency of 1 kHz. However, for the contact force, the peaks consists of few data points. It would be interesting to see whether this is the reason for the differences in the contact force amplitude, due to a time-shift, between the substructured model and the reference model. Since the only nonlinearity during this thesis was based on contact, it would also be interesting to see how well the method works for other forms of nonlinearities such as the nonlinear hooks connecting the panel to the rest of the model.

As the number of retained DOFs showed to have a significant affect of the computational time, applying interface reduction techniques based on generalised DOFs could have a great potential in further increasing the efficiency of the CAE-process.

The results for the substructured model based on "node-to-surface" contact definition showed to predict the contact force amplitudes significantly higher than the reference model. It would also be interesting to see why this is the case.

Bibliography

[1] J. Wijker. *Component Mode Synthesis. In: Mechanical Vibrations in Spacecraft Design.* Springer, Berlin, Heidelberg, 2004, 369-398, DOI: 978-3-662-08587-5.

[2] M. Gibanica. "Experimental-Analytical Dynamic Substructuring". Master's thesis 2013:39, Chalmers University of Technology, 2013.

[3] D. de Klerk, D.J. Rixen and S. N. Voormeeren. General Framework for Dynamic Substructuring: History, Review, and Classification of Techniques. *AIAA Journal* **46**.5 (2008), 1169-1181. DOI:10.2514/1.33274.

[4] *Simulia User Assistance.* Substructures. Version 2017. Dassault Systémes Simulia Corp, 2017.

[5] *MSC Nastran 2018.* Superelements User's Guide. Version 2018.2. MSC, 2018. URL: `https://simcompanion.mscsoftware.com/infocenter/index?page=content&id=DOC11785&cat=MSC_NASTRAN_DOCUMENTATION_2018.2&actp=LIST`.

[6] M. Mohammadali, H. Ahmadian. Efficient model order reduction for dynamic systems with local nonlinearities. *Journal of Sound and Vibration* **333**.6 (2014), 1754-1766. DOI: 10.1016/j.jsv.2013.11.006.

[7] W. Younis. *Up and Running with Autodesk Inventor Simulation 2011, Second Edition.* Butterworth-Heinemann, 2010, 235-275, DOI:10.1016/B978-0-12-382102-7.10009-1.

[8] W. van Drongelen. *Signal Processing for Neuroscientists, Second Edition.* Academic Press, 2018, 103-118, DOI:10.1016/B978-0-12-810482-8.00006-0.

[9] J. W. Cooley, J. W. Tukey. An Algorithm for the Machine Calculation of Complex Fourier Series. *Mathematics of Computation* **19**.90 (1965), 297-301. DOI:10.2307/2003354.

[10] *MATLAB R2018a Documentation,* Version 9.4 `https://se.mathworks.com/help/matlab/`.

[11] T. Irvine. *An introduction to frequency response functions.* (2000) URL: `https://rotorlab.tamu.edu/me617/intro_freq_resp_functions.pdf`.

[12] N. Andersson. "Characterisation of Nonlinear Structural Dynamic Systems in Conceptual Design". PhD thesis, Chalmers University of Technology, 2018. ISBN:978-91-7597-782-9.

[13] SN. Voormeeren. "Dynamic Substructuring Methodologies for Integrated Dynamic Analysis of Wind Turbines". PhD thesis, Delft University of Technology, 2012. ISBN:978-94-91104-10-7.

[14] W. Long. "Model order reduction and substructuring methods for nonlinear structural dynamics". PhD thesis, Delft University of Technology, 2018. ISBN:978-94-6186-935-7.

[15] P. Holzwarth and P. Eberhard. Interface Reduction for CMS Methods and Alternative Model Order Reduction. *IFAC-PapersOnLine* **48**.1 (2015), 254-259. DOI:j.ifacol.2015.05.005.

[16] R. R. Craig and A. J. Kurdila. *Fundamentals of structural dynamics, Second Edition.* Wiley, 2006, ISBN:0-471-43044-7.

[17] J. Schoukens, R. Pintelon and Y. Rolain. *Mastering System Identification in 100 Exercises.* Wiley, 2012, ISBN:978-0-470-93698-6.

[18] T. Abrahamsson. *Calibration and Validation of Structural Dynamics Models.* Chalmers, 2012

[19] C. Mercer. *Acceleration, Velocity and Displacement Spectra – Omega Arithmetic.* Prosig, 2006, URL:`http://prosig.com/wp-content/uploads/pdf/blogArticles/OmegaArithmetic.pdf`.

[20] D. V. Hutton. *Fundamentals of Finite Element Analysis, First Edition.* McGraw-Hill, 2004, ISBN:0-07-239536-2.

[21] Dassault Systémes SolidWorks Corp. *Understanding Nonlinear Analysis.* 2008, URL:`http://nptel.ac.in/courses/105108072/mod07/hyperlink-4.pdf`

[22] M. Mashayekhi. *Comparison of implicit and explicit procedures.* URL: `https://mashayekhi.iut.ac.ir/sites/mashayekhi.iut.ac.ir/files/u32/presentation4.pdf`.

[23] T. Abbey. *Impact, Drop and Crash Testing and Analysis.* DE 247 Digital Engineering, 2013, URL: `https://www.digitalengineering247.com/article/impact-drop-and-crash-testing-and-analysis/`.

[24] A. P. Székely and N. A. Hanna. "Nonlinear Modelling and Simulation of Impact Events and Validation with Experimental Test". Master's thesis, KTH Royal Institute of Technology School of Engineering Sciences, 2018.

[25] M. Bayani. *Internal discussion with PhD student and supervisor Mohsen Bayani. Thesis paper under preparation and is expected to be published by June 2019.*

[26] N. Kikuchi. and J.T. Oden. *Contact problems in elasticity - A study of variational Inequalities and finite element methods.* SIAM, 1988, DOI:10.1137/1.9781611970845.

[27] M. A. BODUR. "Finite element analysis of discontinuous contact problems". Master's thesis, Middle East Technical University, 2006.

[28] Dassault Systémes Simulia Corp *Best Practices for Contact Modeling for Accuracy and Accelerated Convergence.* (2016) - Internal document at VCC.

[29] J. Schoukens and R. Pintelon. *System Identification, A Frequency Domain Approach.* Wiley, 2012, ISBN:978-0-470-64037-1.

[30] M. Bayani, A. P. Szekely, N. Alhanna, H. Viktorsson, C. Wickman, R. Söderberg. Nonlinear modelling and simulation of impact events and validation with physical data, *ISMA*, (2018), ISBN:9789073802995. URL: `urn:nbn:se:kth:diva-246515`.

[31] S. Vizzini. "CMS methods in complete NVH analysis". Master's thesis 2014:50, Chalmers University of Technology, 2014.

[32] M. Gibanica, T. Abrahamsson and D. Rixen. A reduced interface component mode synthesis method using coarse meshes. *Procedia Engineering* **199** (2017) 348-353. DOI:j.proeng.2017.09.031.

A

Appendix 1

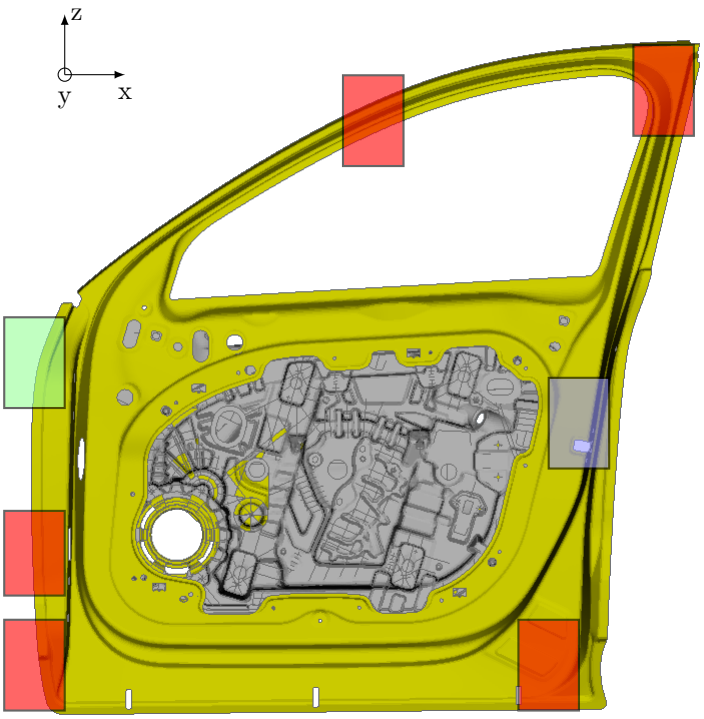

Figure A.1: *Experimental setup of car door, with mounting interface regions marked in red, purple and green. The experimental setup is visualised using the FE-model due to confidentiality.*

B

Appendix 2

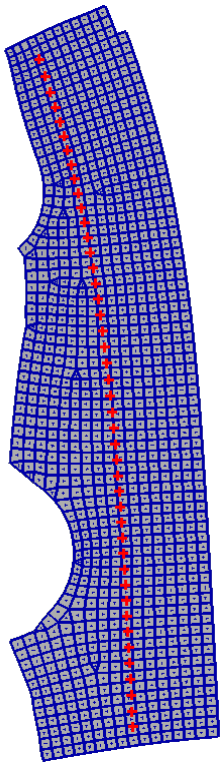

Figure B.1: *Node to surface based contact definition. The nodes highlighted as red crosses represent the node based surface of the panel. These are defined as retained DOFs of the panel substructure. The region highlighted in blue represents the element based contact surface of the frame.*

C
Appendix 3

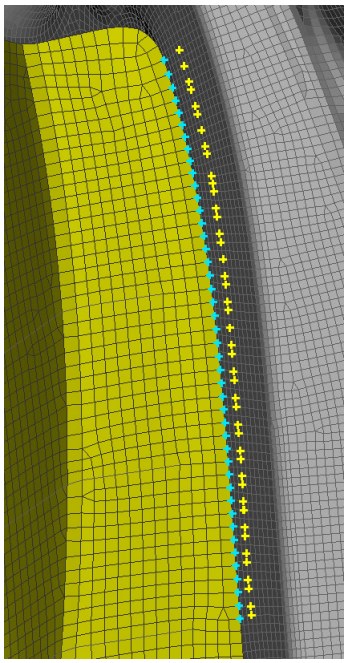

Figure C.1: *Verification node pairs. The slave nodes are highlighted as blue crosses and the master nodes are highlighted as yellow crosses.*